Department of Electrical Engineering and Automation

Model-Based Position Estimation for Synchronous Reluctance Motor Drives

Toni Tuovinen

Aalto University

DOCTORAL DISSERTATIONS

Aalto University publication series
DOCTORAL DISSERTATIONS 86/2014

Model-Based Position Estimation for Synchronous Reluctance Motor Drives

Toni Tuovinen

A doctoral dissertation completed for the degree of Doctor of Science (Technology) to be defended, with the permission of the Aalto University School of Electrical Engineering, at a public examination held at the lecture hall S5 of the school on 20 August 2014 at 12.

Aalto University
School of Electrical Engineering
Department of Electrical Engineering and Automation
Electric Drives

Supervising professors
Prof. Jorma Luomi
Prof. Marko Hinkkanen

Thesis advisor
Prof. Marko Hinkkanen

Preliminary examiners
Prof. Ion Boldea, University Politehnica, Timisoara, Romania
Prof. Maarten Kamper, Stellenbosch University, Matieland, South Africa

Opponent
Prof. Gianmario Pellegrino, Politecnico di Torino, Torino, Italy

Aalto University publication series
DOCTORAL DISSERTATIONS 86/2014

ISBN 978-952-60-5726-2
ISBN 978-952-60-5727-9 (pdf)
ISSN-L 1799-4934
ISSN 1799-4934 (printed)
ISSN 1799-4942 (pdf)
http://urn.fi/URN:ISBN:978-952-60-5727-9

Unigrafia Oy
Helsinki 2014

Finland

441 697
Printed matter

Author
Toni Tuovinen

Name of the doctoral dissertation
Model-Based Position Estimation for Synchronous Reluctance Motor Drives

Publisher School of Electrical Engineering

Unit Department of Electrical Engineering and Automation

Series Aalto University publication series DOCTORAL DISSERTATIONS 86/2014

Field of research Industrial Electronics and Electric Drives

Manuscript submitted 27 March 2014 **Date of the defence** 20 August 2014

Permission to publish granted (date) 13 May 2014 **Language** English

☐ **Monograph** ☒ **Article dissertation (summary + original articles)**

Abstract

This thesis deals with model-based position-estimation methods for synchronous reluctance motor drives. The position estimation methods should be robust against modeling uncertainties, and reliable position information should be obtained at all speeds, including standstill. Since the considered position-estimation methods are model based, methods to obtain the model parameters under normal operation of the drive are proposed.

Three observer structures are studied: a first-order observer, a reduced-order observer and a speed-adaptive full-order observer. The stability of the observers is studied via small-signal linearization under erroneous model parameters. Based on the analysis, robust gain selections are proposed with maximal tolerance for model parameter uncertainties.

For improved performance, the observers are augmented with parameter adaptation laws. The first-order observer and the reduced-order observer are augmented with resistance adaptation laws at low speeds, using information from the back-electromotive force. The speed-adaptive full-order observer is augmented with inductance adaptation law at high speed, using information from the back-electromotive force. At low speeds, the speed-adaptive full-order observer is augmented with resistance adaptation law, using information from high-frequency signal injection. The stability of the augmented observers are studied via small-signal linearization under erroneous model parameters. Based on the analysis, stabilizing gain selections are proposed.

The observers are experimentally evaluated using a 6.7-kW synchronous reluctance motor drive. The first-order observer seems unsuitable for these. The behaviour of the reduced-order observer is closely related to the behaviour of the speed-adaptive full-order observer, but the speed-adaptive full-order observer can be made less sensitive to parameter variations and measurement noise due to the additional degrees of freedom. When the speed-adaptive full-order observer is augmented with parameter-adaptation laws, small position-estimation error is obtained at all speeds, including standstill.

Keywords inductance adaptation, observer, parameter adaptation, sensorless, signal injection stability conditions, resistance adaptation, robustness

ISBN (printed) 978-952-60-5726-2 **ISBN (pdf)** 978-952-60-5727-9

ISSN-L 1799-4934 **ISSN (printed)** 1799-4934 **ISSN (pdf)** 1799-4942

Location of publisher Helsinki **Location of printing** Helsinki **Year** 2014

Pages 136 **urn** http://urn.fi/URN:ISBN:978-952-60-5727-9

A! Aalto-yliopisto

Tiivistelmä

Aalto-yliopisto, PL 11000, 00076 Aalto www.aalto.fi

Tekijä
Toni Tuovinen

Väitöskirjan nimi
Reluktanssitahtimoottorikäyttöjen mallipohjainen asennon estimointi

Julkaisija Sähkötekniikan korkeakoulu

Yksikkö Sähkötekniikan ja automaation laitos

Sarja Aalto University publication series DOCTORAL DISSERTATIONS 86/2014

Tutkimusala Teollisuuselektroniikka ja sähkökäytöt

Käsikirjoituksen pvm 27.03.2014 **Väitöspäivä** 20.08.2014

Julkaisuluvan myöntämispäivä 13.05.2014 **Kieli** Englanti

☐ **Monografia** ☒ **Yhdistelmäväitöskirja (yhteenveto-osa + erillisartikkelit)**

Tiivistelmä

Tämä väitöskirja käsittelee mallipohjaisia menetelmiä reluktanssitahtimoottorikäyttöjen roottorin asennon estimointiin. Estimointimenetelmien tulee olla robusteja mallin parametrivirheille, ja asentotiedon on oltava luotettava kaikilla nopeuksilla. Koska työssä tutkittavat estimointimenetelmät ovat mallipohjaisia, menetelmiä mallien parametrien ajonaikaiselle estimoinnille on ehdotettu.

Työssä on tutkittu kolmea havaitsijarakennetta: ensimmäisen kertaluvun havaitsijaa, vähennetyn kertaluvun havaitsijaa ja adaptiivista täyden kertaluvun havaitsijaa. Havaitsijoiden stabiiliutta on tarkasteltu linearisoidulla piensignaalimallilla mallin parametrien ollessa virheellisiä. Analyysin pohjalta on johdettu havaitsijoiden vahvistuksille ehdot, jotka maksimoivat havaitsijoiden toleranssin parametrivirheille.

Suorituskyvyn parantamiseksi havaitsijoita on laajennettu parametrien adaptointimekanismeilla. Pienillä nopeuksilla ensimmäisen kertaluvun havaitsijaa ja vähennetyn kertaluvun havaitsijaa laajennetaan resistanssin adaptointimekanismilla, joka pohjautuu vastasähkömotoriseen voimaan. Suurilla nopeuksilla täyden kertaluvun havaitsijaa laajennetaan vastasähkömotoriseen voimaan perustuvalla induktanssien adaptoinnilla. Pienillä nopeuksilla täyden kertaluvun havaitsijaa laajennetaan signaali-injektioon perustuvalla resistanssin adaptoinnilla. Laajennettujen havaitsijoiden stabiiliutta on tarkasteltu linearisoidulla piensignaalimallilla mallin parametrien ollessa virheellisiä. Analyysin pohjalta on johdettu havaitsijoiden vahvistuksille stabiilin toiminnan ehdot.

Havaitsijoiden suorituskykyä on arvioitu kokeellisesti 6,7 kW:n reluktanssitahtimoottorikäytöllä. Tulosten perusteella ensimmäisen kertaluvun havaitsija soveltuu huonosti reluktanssitahtimoottoreille. Vähennetyn kertaluvun havaitsija on ominaisuuksiltaan lähellä adaptiivista täyden kertaluvun havaitsijaa, mutta ylimääräisten vapausasteiden vuoksi adaptiivinen täyden kertaluvun havaitsija on vähemmän herkkä parametrivirheille ja mittauskohinalle. Parametrien adaptointimekanismeilla laajennetulla adaptiivisella täyden kertaluvun havaitsijalla saavutetaan pieni estimointivirhe kaikilla nopeuksilla, myös nollanopeudella.

Avainsanat induktanssin adaptointi, havaitsija, parametrien adaptointi, anturiton, signaali-injektio, stabiiliusehdot, resistanssin adaptointi, robustius

ISBN (painettu) 978-952-60-5726-2 **ISBN (pdf)** 978-952-60-5727-9

ISSN-L 1799-4934 **ISSN (painettu)** 1799-4934 **ISSN (pdf)** 1799-4942

Julkaisupaikka Helsinki **Painopaikka** Helsinki **Vuosi** 2014

Sivumäärä 136 **urn** http://urn.fi/URN:ISBN:978-952-60-5727-9

Preface

This dissertation has been done at Aalto University, Department of Electrical Engineering and Automation. The work has been financed by Doctoral Program in Electrical Energy Engineering (DPEEE) and ABB Oy, as a part of an ongoing research project on electric drives.

I started this work under supervision of Prof. Jorma Luomi in 2010. After the sudden demise of Prof. Luomi in 2011 the task of supervising my work was assigned to Prof. Marko Hinkkanen, who was initially the instructor of this work. They both contributed greatly on the writing and outlining of this work, since explicit writing is not quite my forte. I am more fond with equations.

The similar work done by Dr. Antti Piippo on permanent magnet synchronous motors was of great help and served as a convenient starting point. During the years, I have had several constructive advices, and not only related to my work, from both the people working at ABB and from the departmental staff, particularly from the personnel of the electric drives group.

There is always time for more coffee. Or beer.

Espoo, May 28, 2014,

Toni Tuovinen

Contents

List of Publications

This thesis consists of an overview and of the following publications which are referred to in the text by their Roman numerals.

I M. Hinkkanen, T. Tuovinen, L. Harnefors, and J. Luomi. Analysis and design of a position observer with stator-resistance adaptation for PMSM drives. In *International Conference on Electrical Machines (ICEM'10)*, 6 pp., Rome, Italy, September 2010.

II T. Tuovinen, M. Hinkkanen, L. Harnefors, and J. Luomi. A reduced-order position observer with stator-resistance adaptation for synchronous reluctance motor drives. In *International Power Electronics and Motion Control Conference (EPE/PEMC 2010)*, 6 pp., Ohrid, Republic of Macedonia, September 2010.

III Z. Qu, T. Tuovinen and M. Hinkkanen. Inclusion of magnetic saturation in dynamic models of synchronous reluctance motors. In *International Conference on Electrical Machines (ICEM'12)*, pp. 994-1000, Marseille, France, September 2012.

IV T. Tuovinen, M. Hinkkanen, and J. Luomi. Analysis and design of a position observer with resistance adaptation for synchronous reluctance motor drives. *IEEE Transactions on Industry Applications*, vol. 49, issue 1, pp. 66-73, January/February 2013.

V T. Tuovinen, M. Hinkkanen, L. Harnefors, and J. Luomi. Comparison of a reduced-order observer and a full-order observer for sensorless syn-

chronous motor drives. *IEEE Transactions on Industry Applications*, vol. 48, issue 6, pp. 1959-1967, November/December 2012.

VI T. Tuovinen and M. Hinkkanen. Adaptive full-order observer with high-frequency signal injection for synchronous reluctance motor drives. Accepted for publication in *IEEE Journal of Emerging and Selected Topics in Power Electronics*, vol. 2, issue 2, pp. 181-189, June 2014.

VII T. Tuovinen and M. Hinkkanen. Signal-injection assisted full-order observer with parameter adaptation for synchronous reluctance motor drives. Accepted for publication in *IEEE Transactions on Industry Applications*, 12 pp., in press.

Author's Contribution

Publication I: "Analysis and design of a position observer with stator-resistance adaptation for PMSM drives"

The author participated in the writing of the paper and performed the stability evaluations for synchronous reluctance motor drives. Prof. Harnefors contributed by commenting the manuscript.

Publication II: "A reduced-order position observer with stator-resistance adaptation for synchronous reluctance motor drives"

The author wrote the paper under the guidance of Prof. Hinkkanen and Prof. Luomi. Prof. Harnefors contributed by commenting the manuscript.

Publication III: "Inclusion of magnetic saturation in dynamic models of synchronous reluctance motors"

The author performed the measurements and participated in the writing of the paper.

Publication IV: "Analysis and design of a position observer with resistance adaptation for synchronous reluctance motor drives"

The author wrote the paper under the guidance of Prof. Hinkkanen and Prof. Luomi.

Publication V: "Comparison of a reduced-order observer and a full-order observer for sensorless synchronous motor drives"

The author wrote the paper under the guidance of Prof. Hinkkanen and Prof. Luomi. Prof. Harnefors contributed by commenting the manuscript.

Publication VI: "Adaptive full-order observer with high-frequency signal injection for synchronous reluctance motor drives"

The author wrote the paper under the guidance of Prof. Hinkkanen.

Publication VII: "Signal-injection assisted full-order observer with parameter adaptation for synchronous reluctance motor drives"

The author wrote the paper under the guidance of Prof. Hinkkanen.

Symbols

$\mathbf{I}$	Identity matrix
$\boldsymbol{i}_\mathrm{c}$	High-frequency stator-current vector
i_cd	High-frequency direct-axis stator-current component
i_cq	High-frequency quadrature-axis stator-current component
i_d	Direct-axis stator-current component
i_q	Quadrature-axis stator-current component
$\boldsymbol{i}_\mathrm{s}$	Stator-current vector
$\mathbf{J}$	Orthogonal rotation matrix
$\boldsymbol{K}$	Observer gain matrix
k_1	Observer gain
k_{11}	Element of the observer gain matrix $\boldsymbol{K}$
k_{12}	Element of the observer gain matrix $\boldsymbol{K}$
k_2	Observer gain
k_{21}	Element of the observer gain matrix $\boldsymbol{K}$
k_{22}	Element of the observer gain matrix $\boldsymbol{K}$
k_i	Integral gain of the speed adaptation
k_p	Proportional gain of the speed adaptation
$\boldsymbol{L}$	Inductance matrix
$\boldsymbol{L}_\mathrm{c}$	Incremental-inductance matrix
L_d	Direct-axis inductance
L_dd	Direct-axis self-incremental inductance
L_dq	Direct-axis cross-incremental inductance
L_q	Quadrature-axis inductance
L_qd	Quadrature-axis cross-incremental inductance
L_qq	Quadrature-axis self-incremental inductance
R_s	Stator resistance
$\boldsymbol{u}_\mathrm{c}$	High-frequency stator-voltage vector
u_cd	Direct-axis stator-voltage component
u_cq	Quadrature-axis stator-voltage component
u_d	Direct-axis stator-voltage component
u_q	Quadrature-axis stator-voltage component
$\boldsymbol{u}_\mathrm{s}$	Stator-voltage vector

α_{lp}	Bandwidth of the low-pass filter
β	Load parameter ($\beta = i_{\mathrm{q}}/i_{\mathrm{d}}$)
γ_{i}	Integral gain of the signal-injection PI-mechanism
γ_{p}	Proportional gain of the signal-injection PI-mechanism
ϵ	Position-error term in the signal-injection method
ϑ_{m}	Mechanical angular position
$\boldsymbol{\psi}_{\mathrm{s}}$	Stator flux linkage vector
ψ_{d}	Direct-axis stator-flux component
ψ_{q}	Quadrature-axis stator-flux component
ω_{c}	Angular frequency of the signal injection
ω_{ϵ}	Speed-correction term in the signal-injection method
ω_{m}	Angular speed of the rotor

Bold, upper case letter denote matrices, and bold, lower case letters denote vectors. Symbols with circumflex denote estimates, and symbols with tilde denote estimation errors.

1. Introduction

1.1 Background

Synchronous reluctance motors were long considered to be inferior to other electrical motors [Kostko, 1923]. The recent design improvements have increased the torque capabilities and energy efficiency of the synchronous reluctance motors, and due to smaller energy losses modern synchronous reluctance motors can produce 15–20% more torque than induction motors of the same frame size [Boglietti and Pastorelli, 2008]. However, synchronous reluctance motors cannot be started directly from the mains without additional rotor winding.

In order to minimize energy losses and to improve performance of the system, electrical motors are fed with frequency converters in an increasing trend. Utilization of frequency converters actualizes the possibility of replacing the conventional induction motor with synchronous reluctance motor in variable-speed drives. The structure of the synchronous reluctance motor is simpler than that of the induction motor, and due to smaller energy losses the efficiency of the synchronous reluctance motor is larger. Simpler structure and smaller energy losses make synchronous reluctance motors feasible competitors for induction motors.

Simple Volts-per-Hertz control may have unstable operating points when applied for synchronous reluctance motors. Therefore, vector control or direct torque control is usually preferred. In these control methods, information on the rotor position or on the flux angle is needed. The position can be either measured or estimated. Position-sensorless control methods are often preferred, since the mechanical position encoders are expensive and prone to failures. Moreover, in certain conditions mechanical sensors cannot be installed.

The position estimation can be based on the back-electromotive force (back-EMF) induced by the rotational movement of the rotor. The accuracy of these fundamental-excitation-based methods usually relies on parameter-dependent equivalent-circuit models of the motor. Erroneous parameter estimates result in erroneous position estimate, which impairs the stability and performance of the drive. Furthermore, the back-EMF decreases as the speed decreases, and the estimation becomes increasingly sensitive to measurement and modeling errors.

The torque production in synchronous reluctance motors is based on spatially varying reluctance of the rotor. Since the synchronous reluctance motors are inherently salient, methods based on high-frequency excitation can be used to detect the rotor position. Signal-injection methods, however, inflict the system with additional noise and losses.

The magnetic circuit of the synchronous reluctance motors typically saturates strongly under normal operation, i.e. the inductances of the equivalent-circuit model depend on the operation point. Varying model parameters cause inaccurate response, which is a research challenge in sensorless control. Performance of the drive improves, when the saturation is accounted for, and the saturation models can also be utilized in loss-minimization control, for example. Although iron losses and inverter nonlinearities also affect the performance of the drive, these phenomena are not discussed in this thesis.

1.2 Objective and Outline of the Thesis

The objective of this thesis is to develop model-based position-estimation methods for synchronous reluctance motor drives. The focus is on low- and medium-speed operation of the drive. The estimation methods should utilize only measurements available in a typical frequency converter and guarantee stable operation under any practical speed and load conditions. The realizable speed range should span from zero speed at least to the rated speed, and the load range should span at least from zero load to over the rated load. The estimation methods should be robust against parameter variations caused by temperature changes and saturation.

Since the intended position-estimation methods are based on an equivalent-circuit model of the motor, the further aim of this thesis is to develop parameter-estimation methods which can be incorporated in the position-estimation methods. The parameter-estimation methods should

improve the performance of the drive and result in reliable parameter estimates.

The thesis consist of this summary and seven publications. The equivalent-circuit model of the motor, including magnetic saturation, and the experimental setup are described in Chapter 2. Position-estimation methods for synchronous reluctance motor drives are discussed in Chapter 3. On-line parameter-estimation methods are discussed in Chapter 4. The summaries of the publications and the contributions of the thesis are listed in Chapter 5, and Chapter 6 concludes the thesis.

2. System Model

2.1 Fundamental Excitation Model

The synchronous reluctance motor considered in this thesis is assumed to be a symmetrical three-phase system, i.e. the sum of the phase voltages and phase currents is zero. Hence, a two-axis model is sufficient to describe the behaviour of the system. In this thesis, real space vectors will be used. For example, the stator-current vector in the stator-reference frame is $\boldsymbol{i}_{\mathrm{s}}^{\mathrm{s}} = [i_\alpha, i_\beta]^{\mathrm{T}}$, where i_α and i_β are the orthogonal components of the vector, the stator-reference frame is marked with the superscript s, and the matrix transpose is marked with the superscript T. The space-vector representation in the stator-reference frame is obtained from the phase quantities, using Clarke transformation. For example, the stator-current vector is obtained from the phase currents as

$$\begin{bmatrix} i_\alpha \\ i_\beta \end{bmatrix} = \begin{bmatrix} \frac{2}{3} & -\frac{1}{3} & -\frac{1}{3} \\ 0 & \frac{1}{\sqrt{3}} & -\frac{1}{\sqrt{3}} \end{bmatrix} \begin{bmatrix} i_{\mathrm{a}} \\ i_{\mathrm{b}} \\ i_{\mathrm{c}} \end{bmatrix}. \tag{2.1}$$

In order to simplify the analysis, the motor model will be expressed in the estimated rotor reference frame, whose d-axis is aligned at $\hat{\vartheta}_{\mathrm{m}}$ with respect to the stator-reference frame. The electrical position of the actual d-axis is denoted by ϑ_{m}. The d-axis is defined as the direction of the maximum inductance of the rotor. The position depends on the electrical angular rotor speed ω_{m} according to

$$\frac{\mathrm{d}\vartheta_{\mathrm{m}}}{\mathrm{d}t} = \omega_{\mathrm{m}}. \tag{2.2a}$$

The stator-current vector is rotated to the estimated rotor-reference

frame according to

$$\begin{bmatrix} i_\mathrm{d} \\ i_\mathrm{q} \end{bmatrix} = \mathrm{e}^{-\hat{\vartheta}_\mathrm{m}\mathbf{J}} \begin{bmatrix} i_\alpha \\ i_\beta \end{bmatrix} = \left[\cos(-\hat{\vartheta}_\mathrm{m})\mathbf{I} + \sin(-\hat{\vartheta}_\mathrm{m})\mathbf{J}\right] \begin{bmatrix} i_\alpha \\ i_\beta \end{bmatrix}, \tag{2.2b}$$

where the identity matrix and the orthogonal rotation matrix are defined as

$$\mathbf{I} = \begin{bmatrix} 1 & 0 \\ 0 & 1 \end{bmatrix}, \quad \mathbf{J} = \begin{bmatrix} 0 & -1 \\ 1 & 0 \end{bmatrix},$$

respectively. Other space-vector quantities are rotated to the estimated rotor-reference frame in a similar fashion.

The stator inductance is

$$\boldsymbol{L} = \mathrm{e}^{-\tilde{\vartheta}_\mathrm{m}\mathbf{J}} \begin{bmatrix} L_\mathrm{d} & 0 \\ 0 & L_\mathrm{q} \end{bmatrix} \mathrm{e}^{\tilde{\vartheta}_\mathrm{m}\mathbf{J}}, \tag{2.2c}$$

where $\tilde{\vartheta}_\mathrm{m} = \hat{\vartheta}_\mathrm{m} - \vartheta_\mathrm{m}$ is the estimation error in the rotor position, L_d the direct-axis inductance, and L_q the quadrature-axis inductance. The voltage equation is

$$\frac{\mathrm{d}\boldsymbol{\psi}_\mathrm{s}}{\mathrm{d}t} = \boldsymbol{u}_\mathrm{s} - R_\mathrm{s}\boldsymbol{i}_\mathrm{s} - \hat{\omega}_\mathrm{m}\mathbf{J}\boldsymbol{\psi}_\mathrm{s}, \tag{2.2d}$$

where $\boldsymbol{\psi}_\mathrm{s}$ is the stator-flux vector, $\boldsymbol{u}_\mathrm{s}$ the stator-voltage vector, R_s the stator resistance, and $\hat{\omega}_\mathrm{m} = \mathrm{d}\hat{\vartheta}_\mathrm{m}/\mathrm{d}t$ is the angular speed of the coordinate system. The stator current is a nonlinear function

$$\boldsymbol{i}_\mathrm{s} = \boldsymbol{L}^{-1}\boldsymbol{\psi}_\mathrm{s} \tag{2.2e}$$

of the stator-flux vector and the position-estimation error $\tilde{\vartheta}_\mathrm{m}$.

2.2 High-Frequency Model

The high-frequency voltage model is

$$\frac{\mathrm{d}\boldsymbol{\psi}_\mathrm{c}}{\mathrm{d}t} = \boldsymbol{u}_\mathrm{c} - R_\mathrm{s}\boldsymbol{i}_\mathrm{c} - \hat{\omega}_\mathrm{m}\mathbf{J}\boldsymbol{\psi}_\mathrm{c}, \tag{2.3}$$

where $\boldsymbol{\psi}_\mathrm{c}$ is the high-frequency stator-flux vector, $\boldsymbol{u}_\mathrm{c}$ is the high-frequency stator-voltage vector, and $\boldsymbol{i}_\mathrm{c}$ is the high-frequency stator-current vector. The incremental-inductance matrix is

$$\boldsymbol{L}_\mathrm{c} = \mathrm{e}^{-\tilde{\vartheta}_\mathrm{m}\mathbf{J}} \begin{bmatrix} L_\mathrm{dd} & L_\mathrm{dq} \\ L_\mathrm{qd} & L_\mathrm{qq} \end{bmatrix} \mathrm{e}^{\tilde{\vartheta}_\mathrm{m}\mathbf{J}}, \tag{2.4}$$

where the incremental inductances seen by the high-frequency excitation are

$$L_\mathrm{dd} = \frac{\partial\psi_\mathrm{d}}{\partial i_\mathrm{d}}, \quad L_\mathrm{dq} = \frac{\partial\psi_\mathrm{d}}{\partial i_\mathrm{q}}, \quad L_\mathrm{qd} = \frac{\partial\psi_\mathrm{q}}{\partial i_\mathrm{d}}, \quad L_\mathrm{qq} = \frac{\partial\psi_\mathrm{q}}{\partial i_\mathrm{q}}. \tag{2.5}$$

Table 2.1. Per-unit parameters for saturation model.

L_{du}	L_{qu}	α	γ	δ	k	l	m	n
2.73	0.843	0.333	5.58	2.60	6.6	0.8	1	0

Due to reciprocity, $L_{\mathrm{qd}} = L_{\mathrm{dq}}$ will be assumed. It is worth noticing that $L_{\mathrm{qd}} = L_{\mathrm{dq}} = 0$ would hold in the case of no cross-saturation. Furthermore, if the motor did not saturate at all, $L_{\mathrm{dd}} = L_{\mathrm{d}}$ and $L_{\mathrm{qq}} = L_{\mathrm{q}}$ would hold. The high-frequency stator current is a nonlinear function

$$\boldsymbol{i}_{\mathrm{c}} = \boldsymbol{L}_{\mathrm{c}}^{-1}\boldsymbol{\psi}_{\mathrm{c}} \tag{2.6}$$

of the high-frequency stator-flux vector and the position-estimation error $\tilde{\vartheta}_{\mathrm{m}}$. Due to magnetic saturation, $\boldsymbol{L}_{\mathrm{c}}$ depends on the (fundamental) stator current.

The incremental inductances seen in the high-frequency excitation do not necessarily coincide with the incremental inductances seen in the fundamental excitation [de Kock et al., 2007]. The difference between the values measured using the high-frequency signal injection and the values predicted by the fundamental-excitation model originates from iron losses inflicted by the high-frequency signal injection [Lorenz, 2001]. If the frequency of the injected signal were increased, the motor would appear less salient, and eventually position information from the signal injection would be lost.

2.3 Magnetic Saturation

The magnetic saturation model proposed for synchronous reluctance motors in Publication III models the stator current as functions of the estimated flux

$$i_{\mathrm{d}} = \frac{\psi_{\mathrm{d}}}{L_{\mathrm{du}}}\left(1 + \alpha|\psi_{\mathrm{d}}|^{k} + \frac{\delta L_{\mathrm{du}}}{n+2}|\psi_{\mathrm{d}}|^{m}|\psi_{\mathrm{q}}|^{n+2}\right) \tag{2.7a}$$

$$i_{\mathrm{q}} = \frac{\psi_{\mathrm{q}}}{L_{\mathrm{qu}}}\left(1 + \gamma|\psi_{\mathrm{q}}|^{l} + \frac{\delta L_{\mathrm{qu}}}{m+2}|\psi_{\mathrm{d}}|^{m+2}|\psi_{\mathrm{q}}|^{n}\right), \tag{2.7b}$$

where all parameters should be positive. When inductance adaptation was active or experiments on the parameter sensitivity were conducted, the saturation model was not used. The saturation model is not used in the stability analysis. The saturation model parameters are given in Table 2.1.

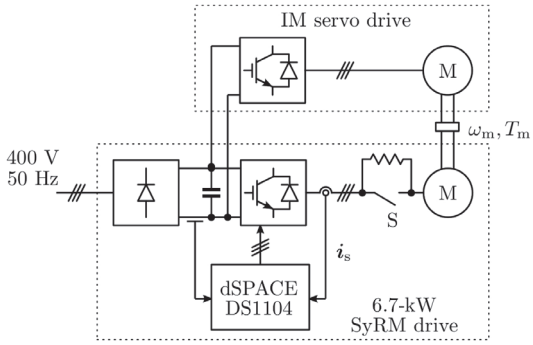

Figure 2.1. Block diagram of the experimental setup used in the laboratory test. The switch S is closed except for the tests conducted in Publication II.

2.4 Experimental Setup and Implementation

The block diagram of the experimental setup is shown in Figure 2.1. The motion-sensorless control system, shown in Figure 2.2, was implemented in a dSPACE DS1104 PPC/DSP board. The control algorithms were implemented using the Matlab/Simulink environment, and the model was compiled and uploaded into the dSPACE board.

A 6.7-kW four-pole SyRM was fed by a frequency converter that is controlled by the DS1104 board. The rated values of the SyRM are: speed 3175 r/min, frequency 105.8 Hz, line-to-line rms voltage 370 V, rms current 15.5 A, and torque 20.1 Nm. The base values for angular speed, voltage and current are defined as $2\pi \cdot 105.8$ rad/s, $\sqrt{2/3} \cdot 370$ V and $\sqrt{2} \cdot 15.5$ A, respectively.

A servo motor was used as a loading machine. The rotor speed ω_m and position ϑ_m were measured using an incremental encoder for monitoring purposes. The shaft torque was measured using a Dataflex 22 torque measuring shaft. The total moment of inertia of the experimental setup is 0.015 kgm^2 (2.7 times the inertia of the SyRM rotor).

The stator currents and the DC-link voltage were measured, and the reference voltage obtained from the current controller was used for the observer as shown in Figure 2.2. The sampling was synchronized to the modulation. The effect of inverter nonlinearities on the stator voltage is substantial at low speeds. Therefore, the most significant inverter nonlinearities, i.e. the dead-time effect and power device voltage drops, have to be compensated for [Pedersen et al., 1993, Choi and Sul, 1996]. Using phase a as an example, a compensated duty cycle for the pulse-width

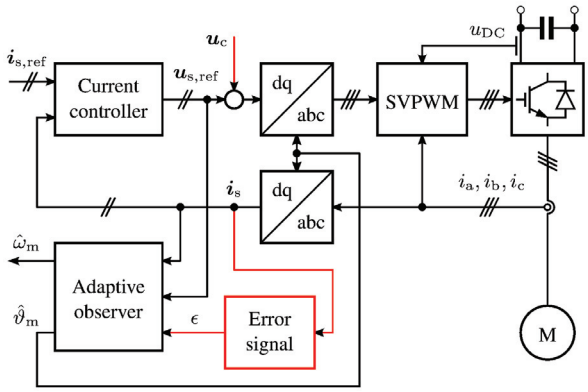

Figure 2.2. Block diagram of the vector control system. The DC-link voltage u_{DC} and the phase currents i_{a}, i_{b}, and i_{c} are measured. The high-frequency voltage excitation $\boldsymbol{u}_{\mathrm{c}}$ is superimposed on the voltage reference. Dead-time effect and power-device voltage drops are compensated for in the space-vector modulator (SVPWM), using the phase-current feedback. The contents of the blocks "Adaptive observer" and "Error signal" are shown in Figures 4.1(a) and 4.1(b), respectively.

modulator was evaluated as

$$d_{\mathrm{a}} = d_{\mathrm{a,ref}} + \frac{2d_\delta}{\pi} \arctan\left(\frac{i_{\mathrm{a}}}{i_\delta}\right), \tag{2.8}$$

where $d_{\mathrm{a,ref}}$ is the ideal duty cycle obtained from the current controller and i_{a} is the phase current. The parameter $d_\delta = 0.009$ p.u. takes into account both the dead-time effect and the threshold voltage of the power devices, while the on-state slope resistance of the power devices is included in the stator-resistance estimate. The shape of the arctan function is determined by the parameter $i_\delta = 0.014$ p.u. The duty cycles of phases b and c were evaluated in a similar manner.

The control system was augmented with a speed controller, whose feedback signal was the speed estimate $\hat{\omega}_{\mathrm{m}}$ obtained from the observer. The stator resistance was estimated via measuring the DC resistance at room temperature.

3. Position Estimation

Since simple Volts-per-Hertz control may have unstable operating points when applied for synchronous reluctance motors [Lipo and Krause, 1967, Cruickshank et al., 1971], field-oriented control is usually preferred in order to achieve higher stability and performance. Field-oriented control requires information on the rotor position or on the flux angle. Although some authors favour stator-flux-oriented control [Kreindler et al., 1993, Lagerquist et al., 1994, Inoue et al., 2010], it was suggested in [Vagati et al., 1997] that the most robust choice for the controllable variables is the d-axis flux ψ_d and the q-axis current i_q, which requires information on the rotor position.

A variety of different methods have been proposed in order to estimate the stator flux angle or the rotor position. The different estimation methods can be roughly divided into two categories: methods which directly utilize the switching states of the frequency converters and methods which are based on the average (effective) voltage of the frequency converter during a switching period. In this thesis, the focus is on methods which are based on the average voltage during pulse-width modulation.

The methods which are based on the average voltage can be roughly divided into two categories: fundamental-excitation methods and signal-injection methods. The methods based on the fundamental excitation (back-electromotive force, back-EMF) are relatively simple and provide satisfactory accuracy at medium and high speeds. However, the back-EMF decreases as the speed decreases, and the disrupting effects of modeling errors and system noise increase, which may render the back-EMF methods inoperable at low speeds.

Due to the inherent saliency of the synchronous reluctance motors, methods based on high-frequency excitation can be used to detect the ro-

tor position at all speed, including standstill. Because the signal-injection methods inflict the system with additional noise and losses, combined approaches can be used. These rely on signal injection near standstill, and back-EMF-based methods dominate at higher speeds.

In this thesis, three back-EMF-based observer structures, with increasing complexity, are investigated for rotor-position estimation. Since the investigated estimation methods are model based, the accuracy and stability of the drive depends on the accuracy of the equivalent-circuit model parameters. For improved performance, the main focus has been on stability analysis with uncertain model parameter estimates. Speed-estimation methods have been briefly addressed with the related position-estimation methods. If the drive is operated in torque-control mode, speed estimation is not mandatory.

3.1 Current-Slope Methods

The estimation methods which rely on the behaviour of the system during switching states of the frequency converter are natural choices for direct torque controlled (DTC) drives. These methods are based on measuring the slopes of the phase currents during switching states. In [Matsuo and Lipo, 1995], the position information is extracted from the current ripples in hysteresis current control. The method requires look-up tables for the rate of change of the currents as functions of the position. Similar approaches have been addressed in [Xiang and Nasar, 1995] and [Jovanović et al., 1998]. In the latter case, the quality of the speed estimate is improved using an angular velocity observer introduced in [Lorenz and Patten, 1991].

In order to eliminate the need for preliminary measurements, the method proposed in [Schroedl and Weinmeier, 1994] applies test-voltage injections in two different directions, and the position information can be extracted from the measured currents without voltage measurements or knowledge of the motor parameters. However, since the quality of this position-estimation method declines as the rotational speed increases, a back-EMF-based observer is used at high speeds. Since the direct calculation of position and speed from measured currents results in noisy estimates, Kalman filters have been applied in order to obtain usable position and speed estimates.

The method has been further improved to cover the entire operation

range in [Chen et al., 2004] and [Wei and Liu, 2012], using single and dual current-slope techniques, respectively, without additional test signals. Similar approaches for DTC drives have been proposed in [Morales-Caporal and Pacas, 2008], where additional test voltage signals are injected during zero voltage of DTC, and in [Landsmann et al., 2010a], where normal operation of predictive DTC is utilized.

3.2 Fundamental-Excitation Methods

3.2.1 Voltage Models

The most important system state in the field-oriented control is the rotor position (or the flux angle). Various approaches have been proposed to extract the position information from the back-EMF, of which some methods require information on the equivalent-circuit model parameters. Simplest methods rely directly on current or voltage measurements, without knowledge on the model parameters.

A simple model-independent approach was introduced in [Kreindler et al., 1993], where the position information was obtained via tracking the zero crossings of the third harmonic of the phase voltages in a saturated motor. The method, however, requires access to the neutral point, which is not always available. Somewhat related approach was used in [Arefeen et al., 1994], where the current in one phase was kept at zero after zero crossing and test signals were injected to the other phases. The voltage induced to the phase with current kept at zero was measured, and the position was determined based on a look-up table. Both these methods provide effectively only six position samples per electrical cycle, which leads to only moderate performance.

A simple model-dependent position-estimation method was introduced in [Stumper et al., 2010]. The method is based on calculating the rotor position directly from instantaneous voltages and currents. The method provides directly only position estimates between $-\pi/4$ and $3\pi/4$. Thus, a low-pass filter is used in order to extend the estimator range to cover the entire operation range,

$$\frac{\mathrm{d}\hat{\vartheta}_\mathrm{m}}{\mathrm{d}t} = -\alpha \left[(\hat{\vartheta}_\mathrm{m} \bmod \pi) - \hat{\vartheta}'_\mathrm{m} \right], \tag{3.1}$$

where α is the position-estimation bandwidth, $\hat{\vartheta}'_\mathrm{m}$ is the position information from the direct estimation, mod is the modulo operation, and $\hat{\vartheta}_\mathrm{m}$ is

the usable position information. The necessary parameters used in this method are the stator resistance and the average stator inductance.

In [Lagerquist et al., 1994], the stator-flux estimate was obtained via integrating the voltage equation in the stator-reference frame,

$$\frac{\mathrm{d}\hat{\boldsymbol{\psi}}_\mathrm{s}^\mathrm{s}}{\mathrm{d}t} = \boldsymbol{u}_\mathrm{s}^\mathrm{s} - \hat{R}_\mathrm{s}\boldsymbol{i}_\mathrm{s}^\mathrm{s}, \tag{3.2}$$

where $\hat{R}_\mathrm{s}$ is the stator-resistance estimate. The flux angle was extracted from the estimated flux components

$$\hat{\vartheta} = \arctan\left(\frac{\hat{\psi}_\beta}{\hat{\psi}_\alpha}\right), \tag{3.3}$$

where $\hat{\psi}_\alpha$ and $\hat{\psi}_\beta$ are the estimated stator-flux components in the stator-reference frame. No information on the rotor position is available. The speed estimate was obtained directly from the flux angle estimate as

$$\hat{\omega}_\mathrm{m} = \frac{\mathrm{d}\hat{\vartheta}}{\mathrm{d}t}. \tag{3.4}$$

In transient states, this leads to poor speed-estimation dynamics. Hence, the torque dynamics has to be limited if reliable speed estimation is desired. Similar approach to estimate the stator flux at high speeds was used in [Ha et al., 1999], where the rotor position is estimated from the flux angle as

$$\hat{\vartheta}_\mathrm{m} = \arctan\left(\frac{\hat{\psi}_\beta}{\hat{\psi}_\alpha}\right) - \arctan\left(\frac{\hat{L}_\mathrm{q} i_\mathrm{q}}{\hat{L}_\mathrm{d} i_\mathrm{d}}\right), \tag{3.5}$$

where $\hat{L}_\mathrm{d}$ and $\hat{L}_\mathrm{q}$ are the direct-axis and quadrature-axis inductance estimates, respectively.

Due to measurement noise and bias, the pure voltage integration without corrections as in (3.2) is prone to drift. A simple improvement is to replace the pure integration with low-pass filters as in [Ghaderi and Hanamoto, 2011]. Another approach is to introduce a feedback to the voltage integration. Different feedback methods have been used in [Capecchi et al., 2001] and [Agarlită et al., 2012], for example, which are both based on measured behaviour of the stator flux as function of the stator current, i.e. $\boldsymbol{\psi}_\mathrm{s} = \boldsymbol{\psi}_\mathrm{s}(\boldsymbol{i}_\mathrm{s})$. In [Capecchi et al., 2001], the stator flux is estimated as

$$\frac{\mathrm{d}\hat{\boldsymbol{\psi}}_\mathrm{s}^\mathrm{su}}{\mathrm{d}t} = \boldsymbol{u}_\mathrm{s}^\mathrm{s} - \hat{R}_\mathrm{s}\boldsymbol{i}_\mathrm{s}^\mathrm{s} + g\left(\hat{\boldsymbol{\psi}}_\mathrm{s}^\mathrm{si} - \hat{\boldsymbol{\psi}}_\mathrm{s}^\mathrm{su}\right), \tag{3.6}$$

where $\hat{\boldsymbol{\psi}}_\mathrm{s}^\mathrm{si}$ is based on the measured behaviour of $\boldsymbol{\psi}_\mathrm{s}(\boldsymbol{i}_\mathrm{s})$ and g is a design parameter associated with the crossover frequency between the pure

voltage integration and the current based model $\hat{\boldsymbol{\psi}}_\mathrm{s}^\mathrm{si}$. The slightly different approach in [Agarlită et al., 2012] introduces a compensation voltage vector

$$\boldsymbol{v}_\mathrm{c} = k_\mathrm{p}\tilde{\boldsymbol{\psi}}_\mathrm{s} + \int k_\mathrm{i}\tilde{\boldsymbol{\psi}}_\mathrm{s}\mathrm{d}t, \tag{3.7}$$

where k_p and k_i are adaptation gains and $\tilde{\boldsymbol{\psi}}_\mathrm{s} = \hat{\boldsymbol{\psi}}_\mathrm{s}^\mathrm{su} - \hat{\boldsymbol{\psi}}_\mathrm{s}^\mathrm{si}$. The compensation voltage vector is incorporated in the voltage integration

$$\frac{\mathrm{d}\hat{\boldsymbol{\psi}}_\mathrm{s}^\mathrm{su}}{\mathrm{d}t} = \boldsymbol{u}_\mathrm{s}^\mathrm{s} - \hat{R}_\mathrm{s}\boldsymbol{i}_\mathrm{s}^\mathrm{s} + \boldsymbol{v}_\mathrm{c}. \tag{3.8}$$

In both these approaches, the flux estimation is dominated by the measured $\boldsymbol{\psi}_\mathrm{s}(\boldsymbol{i}_\mathrm{s})$ characteristics at low speeds, and the pure voltage integration dominates at high speeds. Since the $\boldsymbol{\psi}_\mathrm{s}(\boldsymbol{i}_\mathrm{s})$ characteristics are determined in the dq-frame, a rotor-position estimate is required. In [Capecchi et al., 2001], the trigonometric functions needed for the coordinate transformation were calculated utilizing the flux estimates both in the $\alpha\beta$-frame and the dq-frame,

$$\sin\hat{\vartheta}_\mathrm{m} = \frac{\tilde{\psi}_\mathrm{d}\hat{\psi}_\beta - \hat{\psi}_\alpha\tilde{\psi}_\mathrm{q}}{\hat{\psi}_\mathrm{s}^2}, \quad \cos\hat{\vartheta}_\mathrm{m} = \frac{\tilde{\psi}_\mathrm{d}\hat{\psi}_\alpha + \hat{\psi}_\beta\tilde{\psi}_\mathrm{q}}{\hat{\psi}_\mathrm{s}^2}, \tag{3.9}$$

where $\hat{\psi}_\mathrm{s}$ is the magnitude of the estimated stator flux. The speed estimate was obtained directly from the time derivatives of $\cos\hat{\vartheta}_\mathrm{m}$ and $\sin\hat{\vartheta}_\mathrm{m}$,

$$\hat{\omega}_\mathrm{m} = \cos\hat{\vartheta}_\mathrm{m}\frac{\mathrm{d}\sin\hat{\vartheta}_\mathrm{m}}{\mathrm{d}t} - \sin\hat{\vartheta}_\mathrm{m}\frac{\mathrm{d}\cos\hat{\vartheta}_\mathrm{m}}{\mathrm{d}t}, \tag{3.10}$$

while the final speed and position estimation from the noisy flux estimates in [Agarlită et al., 2012] was based on the work presented in [Lorenz and Patten, 1991].

The approach used in [Ichikawa et al., 2003] was based on the extended-EMF (EEMF) concept. Only the EEMF part of the voltage equation depends on the rotor position,

$$\boldsymbol{v}_\mathrm{e} = (L_\mathrm{d} - L_\mathrm{q})\left(\omega_\mathrm{m}i_\mathrm{d} - \frac{\mathrm{d}i_\mathrm{q}}{\mathrm{d}t}\right)\begin{bmatrix}-\sin(\vartheta_\mathrm{m})\\ \cos(\vartheta_\mathrm{m})\end{bmatrix}. \tag{3.11}$$

The EEMF was estimated using a reduced-order observer, and the rotor position estimate was extracted directly from the estimated EEMF,

$$\hat{\vartheta}_\mathrm{m} = \arctan\left(\frac{-\hat{v}_{\mathrm{e},\alpha}}{\hat{v}_{\mathrm{e},\beta}}\right). \tag{3.12}$$

The speed was estimated using an adaptive velocity estimator based on the work presented in [Tomita et al., 1998].

Slightly different approach used in [Landsmann et al., 2010b] was based on estimating only the position-dependent part of the stator flux

$$\boldsymbol{\psi}_{\Delta}^{\mathrm{s}} = \frac{L_{\mathrm{d}} - L_{\mathrm{q}}}{2} \begin{bmatrix} \cos(2\vartheta_{\mathrm{m}}) & \sin(2\vartheta_{\mathrm{m}}) \\ \sin(2\vartheta_{\mathrm{m}}) & -\cos(2\vartheta_{\mathrm{m}}) \end{bmatrix} \boldsymbol{i}_{\mathrm{s}}^{\mathrm{s}}. \tag{3.13}$$

Feedback from the estimated position-dependent flux component was used to compensate the integration drift,

$$\hat{\boldsymbol{\psi}}_{\Delta}^{\mathrm{s}} = \int \left(\boldsymbol{u}_{\mathrm{s}}^{\mathrm{s}} - \hat{R}_{\mathrm{s}} \boldsymbol{i}_{\mathrm{s}}^{\mathrm{s}} - k_{\mathrm{d}} \hat{\boldsymbol{\psi}}_{\Delta}^{\mathrm{s}} \right) \mathrm{d}t - \frac{\hat{L}_{\mathrm{d}} + \hat{L}_{\mathrm{q}}}{2} \boldsymbol{i}_{\mathrm{s}}^{\mathrm{s}}, \tag{3.14}$$

where k_{d} is the feedback gain. The position-estimation error was obtained from the cross product

$$\epsilon = \left(\hat{\boldsymbol{\psi}}_{\Delta}^{\mathrm{s}} \right)^{\mathrm{T}} \mathbf{J} \hat{\boldsymbol{\psi}}_{\Delta}^{\mathrm{si}}, \tag{3.15}$$

where $\hat{\boldsymbol{\psi}}_{\Delta}^{\mathrm{si}}$ is based on the measured behaviour of $\boldsymbol{\psi}_{\mathrm{s}}(\boldsymbol{i}_{\mathrm{s}})$. The error signal ϵ was driven to zero with a PI-mechanism.

3.2.2 Simple Observer

The simple observer considered in Publication I for permanent-magnet synchronous motor drives is derived by expressing the back-EMF in two different ways. For synchronous reluctance motors, these can be expressed as

$$\hat{\boldsymbol{e}} = \hat{\omega}_{\mathrm{m}} \mathbf{J} \hat{\boldsymbol{L}} \boldsymbol{i}_{\mathrm{s}} \tag{3.16a}$$

$$\boldsymbol{e}' = \boldsymbol{u}_{\mathrm{s}} - \hat{R}_{\mathrm{s}} \boldsymbol{i}_{\mathrm{s}} - \hat{\boldsymbol{L}} \frac{\mathrm{d}\boldsymbol{i}_{\mathrm{s}}}{\mathrm{d}t}, \tag{3.16b}$$

where the model inductance matrix is

$$\hat{\boldsymbol{L}} = \begin{bmatrix} \hat{L}_{\mathrm{d}} & 0 \\ 0 & \hat{L}_{\mathrm{q}} \end{bmatrix}. \tag{3.17}$$

The observer is composed from (3.16) as

$$\boldsymbol{k}^{\mathrm{T}} (\hat{\boldsymbol{e}} - \boldsymbol{e}') = 0, \tag{3.18}$$

where $\boldsymbol{k} = [g, 1]^T$ is a projection vector and g is the observer gain. The speed estimate can be solved as

$$\hat{\omega}_{\mathrm{m}} = \frac{\boldsymbol{k}^T (\boldsymbol{u}_{\mathrm{s}} - \hat{R}_{\mathrm{s}} \boldsymbol{i}_{\mathrm{s}} - \hat{\boldsymbol{L}} \frac{\mathrm{d}\boldsymbol{i}_{\mathrm{s}}}{\mathrm{d}t})}{\boldsymbol{k}^T \mathbf{J} \hat{\boldsymbol{L}} \boldsymbol{i}_{\mathrm{s}}}. \tag{3.19}$$

In component form, this gives

$$\hat{\omega}_{\mathrm{m}} = \frac{u_{\mathrm{q}} - \hat{R}_{\mathrm{s}} i_{\mathrm{q}} - \hat{L}_{\mathrm{q}} \frac{\mathrm{d}i_{\mathrm{q}}}{\mathrm{d}t} + g(u_{\mathrm{d}} - \hat{R}_{\mathrm{s}} i_{\mathrm{d}} - \hat{L}_{\mathrm{d}} \frac{\mathrm{d}i_{\mathrm{d}}}{\mathrm{d}t})}{\hat{L}_{\mathrm{d}} i_{\mathrm{d}} - g \hat{L}_{\mathrm{q}} i_{\mathrm{q}}}. \tag{3.20}$$

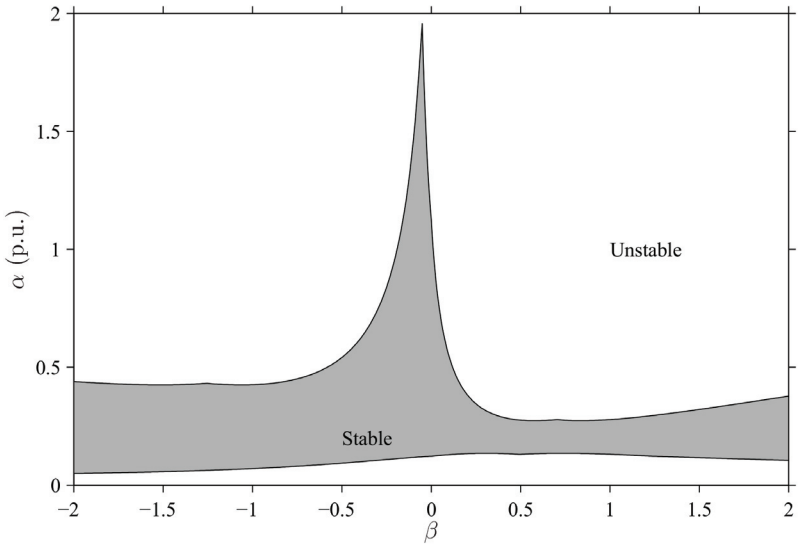

Figure 3.1. Stablity map of the simple observer with 20% parameter uncertainties and $\hat{\omega}_\mathrm{m} = 0.1$ p.u. Stable area is shaded and unstable areas are blank.

The position estimate is obtained from integrating (3.19),

$$\hat{\vartheta}_\mathrm{m} = \int \hat{\omega}_\mathrm{m} \mathrm{d}t. \tag{3.21}$$

The steady-state position-estimation error $\tilde{\vartheta}_\mathrm{m0}$ of the closed-loop system consisting of (2.2) and (3.19) is determined by

$$A\cos 2\tilde{\vartheta}_\mathrm{m0} + B\sin 2\tilde{\vartheta}_\mathrm{m0} + C = 0, \tag{3.22a}$$

where

$$A = (L_\mathrm{d} - L_\mathrm{q})(1 + g\beta) \tag{3.22b}$$

$$B = -(L_\mathrm{d} - L_\mathrm{q})(\beta - g) \tag{3.22c}$$

$$C = 2\tilde{L}_\mathrm{d} + 2g\beta\tilde{L}_\mathrm{q} - 2(\beta + g)\frac{\tilde{R}_\mathrm{s}}{\hat{\omega}_\mathrm{m}} - A \tag{3.22d}$$

and $\beta = i_\mathrm{q}/i_\mathrm{d}$, $\tilde{R}_\mathrm{s} = \hat{R}_\mathrm{s} - R_\mathrm{s}$, $\tilde{L}_\mathrm{d} = \hat{L}_\mathrm{d} - L_\mathrm{d}$ and $\tilde{L}_\mathrm{q} = \hat{L}_\mathrm{q} - L_\mathrm{q}$. The solution for the steady-state position-estimation error is

$$\tilde{\vartheta}_\mathrm{m0} = -\frac{\arcsin\left(\frac{C}{D}\right) + \phi}{2}, \tag{3.23a}$$

where

$$\phi = \arctan\left(\frac{A}{B}\right), \quad D = \frac{B}{\cos\phi}. \tag{3.23b}$$

The linearization of (2.2) and (3.19) with respect to $\tilde{\vartheta}_\mathrm{m}$ results in

$$\frac{\mathrm{d}\tilde{\vartheta}_\mathrm{m}}{\mathrm{d}t} = \hat{\omega}_\mathrm{m0}\frac{\boldsymbol{k}^T\mathbf{J}\frac{\mathrm{d}\boldsymbol{L}}{\mathrm{d}\tilde{\vartheta}_\mathrm{m}}\boldsymbol{i}_\mathrm{s}}{\boldsymbol{k}^T(\mathbf{J}\hat{\boldsymbol{L}} - \boldsymbol{L}\mathbf{J})\boldsymbol{i}_\mathrm{s}}\tilde{\vartheta}_\mathrm{m}, \tag{3.24}$$

where $\hat{\omega}_{\mathrm{m}0}$ is the steady-state operating-point value of $\hat{\omega}_{\mathrm{m}}$. This can be expressed in the form

$$\frac{\mathrm{d}\tilde{\vartheta}_{\mathrm{m}}}{\mathrm{d}t} = -\alpha\tilde{\vartheta}_{\mathrm{m}}, \tag{3.25}$$

where α is the position-estimation bandwidth. With accurate parameter estimates, the observer gain selection can be expressed as

$$g = \frac{\beta\hat{\omega}_{\mathrm{m}} - \alpha}{\beta\alpha + \hat{\omega}_{\mathrm{m}}}. \tag{3.26}$$

As the load varies, it is difficult to choose α in such a way that the gain g remains small, i.e. $|\beta\alpha + \hat{\omega}_{\mathrm{m}}|$ is sufficiently larger than zero, and at the same time has relatively fast position estimation.

The robustness of the simple observer is studied using the linearized estimation-error dynamics given in (3.24) after the steady-state estimation error was solved using (3.23). The steady-state operation with β varying from -2 to 2 at $\hat{\omega}_{\mathrm{m}0} = 0.1$ p.u. was considered. The actual parameters correspond to those of the 6.7-kW SyRM: L_{d} = 2.00 p.u., L_{q} = 0.3 p.u. and R_{s} = 0.042 p.u. The same relative uncertainty (20%) is assumed for all three model parameters $\hat{L}_{\mathrm{d}}$, $\hat{L}_{\mathrm{q}}$ and $\hat{R}_{\mathrm{s}}$. Hence, eight different worst-case combinations, consisting of minimum and maximum values of the model parameters, can be formed. For example, one of the worst-case combinations is $\hat{L}_{\mathrm{d}} = 0.8L_{\mathrm{d}}$, $\hat{L}_{\mathrm{q}} = 1.2L_{\mathrm{q}}$ and $\hat{R}_{\mathrm{s}} = 0.8R_{\mathrm{s}}$. At each studied operating point, the local stability of the system was analyzed for all eight worst-case combinations of erroneous model parameters.

The stability of the estimation-error dynamics with erroneous model parameters was tested for different values of the design parameter α. The stability map is depicted in Figure 3.1, where the stable area is shaded and the unstable areas are blank. It can be seen that the stable region in the motoring mode is very narrow, particularly near $\beta = 0.5$. Due to high sensitivity to parameter errors and difficulties in gain selection, the method was deemed insufficient for synchronous reluctance motor drives.

3.2.3 Reduced-Order Observer

The reduced-order observer considered in Publication II consists of estimating the d-axis flux component together with the rotor position,

$$\frac{\mathrm{d}\hat{\psi}_{\mathrm{d}}}{\mathrm{d}t} = u_{\mathrm{d}} - \hat{R}_{\mathrm{s}}i_{\mathrm{d}} + \hat{\omega}_{\mathrm{m}}\hat{L}_{\mathrm{q}}i_{\mathrm{q}} + k_1(\hat{\psi}_{\mathrm{d}} - \hat{L}_{\mathrm{d}}i_{\mathrm{d}}) \tag{3.27a}$$

$$\frac{\mathrm{d}\hat{\vartheta}_{\mathrm{m}}}{\mathrm{d}t} = \frac{u_{\mathrm{q}} - \hat{R}_{\mathrm{s}}i_{\mathrm{q}} - \hat{L}_{\mathrm{q}}\frac{\mathrm{d}i_{\mathrm{q}}}{\mathrm{d}t} + k_2(\hat{\psi}_{\mathrm{d}} - \hat{L}_{\mathrm{d}}i_{\mathrm{d}})}{\hat{\psi}_{\mathrm{d}}} = \hat{\omega}_{\mathrm{m}}, \tag{3.27b}$$

where k_1 and k_2 are observer gains. The observer utilizes feedback from the flux-estimation error in the d-axis direction only. The nonlinear estimation error dynamics of the closed-loop system consisting of (2.2) and (3.27) are

$$\frac{\mathrm{d}\tilde{\boldsymbol{\psi}}_\mathrm{s}}{\mathrm{d}t} = (\boldsymbol{K}\hat{\boldsymbol{L}}^{-1} - \hat{\omega}_\mathrm{m}\mathbf{J})\tilde{\boldsymbol{\psi}}_\mathrm{s} + \left[\boldsymbol{K}(\hat{\boldsymbol{L}}^{-1}\boldsymbol{L} - \mathbf{I}) - \tilde{R}_\mathrm{s}\right]\boldsymbol{i}_\mathrm{s}, \tag{3.28a}$$

where $\tilde{\boldsymbol{\psi}}_\mathrm{s} = \hat{\boldsymbol{\psi}}_\mathrm{s} - \boldsymbol{\psi}_\mathrm{s}$ and the gain matrix $\boldsymbol{K}$ utilizes the flux-estimation error only in the d-axis direction in accordance with (3.27),

$$\boldsymbol{K} = \begin{bmatrix} k_1\hat{L}_\mathrm{d} & 0 \\ k_2\hat{L}_\mathrm{d} & 0 \end{bmatrix}. \tag{3.28b}$$

The gains are scaled with $\hat{L}_\mathrm{d}$ in order to simplify the notation in the following analysis.

The error of the q-axis flux is a nonlinear function of the position-estimation error, since $\hat{\psi}_\mathrm{q} = \hat{L}_\mathrm{q} i_\mathrm{q}$ and

$$\psi_\mathrm{q} = \frac{i_\mathrm{q}}{2}(L_\mathrm{d} + L_\mathrm{q}) - \frac{i_\mathrm{d}}{2}(L_\mathrm{d} - L_\mathrm{q})\left[\sin(2\tilde{\vartheta}_\mathrm{m}) + \beta\cos(2\tilde{\vartheta}_\mathrm{m})\right], \tag{3.28c}$$

which can be obtained from (2.2e).

The steady-state position-estimation error is determined by

$$A\cos 2\tilde{\vartheta}_\mathrm{m0} + B\sin 2\tilde{\vartheta}_\mathrm{m0} + C = 0, \tag{3.29a}$$

where

$$A = (L_\mathrm{d} - L_\mathrm{q})\left[\beta(k_2 - \hat{\omega}_\mathrm{m0}) - k_1\right] \tag{3.29b}$$

$$B = (L_\mathrm{d} - L_\mathrm{q})\left[(k_2 - \hat{\omega}_\mathrm{m0}) + \beta k_1\right] \tag{3.29c}$$

$$C = 2k_1\tilde{L}_\mathrm{d} + 2\beta(k_2 - \hat{\omega}_\mathrm{m0})\tilde{L}_\mathrm{q} - 2\left(k_2 - \hat{\omega}_\mathrm{m0} - \beta k_1\right)\frac{\tilde{R}_\mathrm{s}}{\hat{\omega}_\mathrm{m0}} - A. \tag{3.29d}$$

The solution for the steady-state position-estimation error is obtained in a fashion similar to (3.23).

After the steady-state estimation errors have been solved, (3.28a) is linearized in the vicinity of these steady-state errors, which yields

$$\frac{\mathrm{d}}{\mathrm{d}t}\begin{bmatrix}\tilde{\psi}_\mathrm{d} \\ \tilde{\psi}_\mathrm{q}\end{bmatrix} = \begin{bmatrix} k_1 & \hat{\omega}_\mathrm{m0} - k_1\beta' \\ k_2 - \hat{\omega}_\mathrm{m0} & -k_2\beta' \end{bmatrix}\begin{bmatrix}\tilde{\psi}_\mathrm{d} \\ \tilde{\psi}_\mathrm{q}\end{bmatrix}, \tag{3.30}$$

where

$$\beta' = \tan(2\tilde{\vartheta}_\mathrm{m0} + \arctan\beta). \tag{3.31}$$

The characteristic polynomial of (3.30) is

$$s^2 + b's + c', \tag{3.32}$$

where

$$b' = k_2\beta' - k_1 \tag{3.33a}$$

$$c' = \hat{\omega}_{\mathrm{m}0}^2 - \hat{\omega}_{\mathrm{m}0}\left(k_2 + k_1\beta'\right). \tag{3.33b}$$

In order to stabilize the system, b' and c' should be positive.

If accurate motor parameters are assumed, then the gains k_1 and k_2 can be solved from (3.33) as functions of the coefficients of the characteristic polynomial $b' = b$ and $c' = c$. The coefficients b and c can be regarded as design parameters, and the gains are

$$k_1 = -\frac{b + \beta(c/\hat{\omega}_{\mathrm{m}} - \hat{\omega}_{\mathrm{m}})}{\beta^2 + 1}, \quad k_2 = \frac{\beta b - c/\hat{\omega}_{\mathrm{m}} + \hat{\omega}_{\mathrm{m}}}{\beta^2 + 1}. \tag{3.34}$$

With accurate parameter estimates, the system is stable for all positive values of b and c.

It was pointed out in Publication IV and Publication V that the reduced-order observer is relatively sensitive to harmonic noise and parameter uncertainties. Hence, a speed-adaptive full-order observer was considered in Publication VI and Publication VII.

3.2.4 Speed-Adaptive Full-Order Observer

In the speed-adaptive full-order observer, the stator-flux vector is estimated according to

$$\frac{\mathrm{d}\hat{\boldsymbol{\psi}}_{\mathrm{s}}}{\mathrm{d}t} = \boldsymbol{u}_{\mathrm{s}} - \hat{R}_{\mathrm{s}}\hat{\boldsymbol{i}}_{\mathrm{s}} - \hat{\omega}_{\mathrm{m}}\mathbf{J}\hat{\boldsymbol{\psi}}_{\mathrm{s}} + \boldsymbol{K}\tilde{\boldsymbol{i}}_{\mathrm{s}} \tag{3.35a}$$

$$\hat{\boldsymbol{i}}_{\mathrm{s}} = \hat{\boldsymbol{L}}^{-1}\hat{\boldsymbol{\psi}}_{\mathrm{s}}, \tag{3.35b}$$

where $\tilde{\boldsymbol{i}}_{\mathrm{s}} = \hat{\boldsymbol{i}}_{\mathrm{s}} - \boldsymbol{i}_{\mathrm{s}}$. In order to simplify the analysis, the observer gain matrix is written –without loss of generality– as

$$\boldsymbol{K} = \begin{bmatrix} \hat{R}_{\mathrm{s}} + \hat{L}_{\mathrm{d}}k_{11} & \hat{L}_{\mathrm{q}}k_{12} \\ \hat{L}_{\mathrm{d}}k_{21} & \hat{R}_{\mathrm{s}} + \hat{L}_{\mathrm{q}}k_{22} \end{bmatrix}. \tag{3.35c}$$

The rotor speed is adapted using the PI-mechanism

$$\hat{\omega}_{\mathrm{m}} = k_{\mathrm{p}}\tilde{i}_{\mathrm{q}} + \int k_{\mathrm{i}}\tilde{i}_{\mathrm{q}}\mathrm{d}t, \tag{3.35d}$$

and the rotor position is obtained according to (3.21).

Since the speed-adaptation law drives $\tilde{i}_{\mathrm{q}}$ to zero, the adaptation gains k_{p} and k_{i} do not affect the position-estimation error in the steady state, and the equation for the steady-state position-estimation error is the same as for the reduced-order observer, i.e. (3.29).

If the gains k_{12} and k_{22} in (3.35c) are selected according to

$$k_{12} = -\beta k_{11} \tag{3.36a}$$

$$k_{22} = -\beta k_{21} \tag{3.36b}$$

then with accurate parameter estimates the dynamics of the speed-adaptation loop are disconnected from the dynamics of the flux observer. Furthermore, if the speed-adaptation gains are selected as

$$k_{\mathrm{p}} = \frac{\hat{L}_{\mathrm{q}} d}{(\hat{L}_{\mathrm{d}} - \hat{L}_{\mathrm{q}}) i_{\mathrm{d}}}, \quad k_{\mathrm{i}} = \frac{\hat{L}_{\mathrm{q}} e}{(\hat{L}_{\mathrm{d}} - \hat{L}_{\mathrm{q}}) i_{\mathrm{d}}} \tag{3.37}$$

and the flux-observer gains are selected as

$$k_{11} = k_1, \quad k_{21} = k_2, \tag{3.38}$$

where k_1 and k_2 are defined in (3.34), the characteristic polynomial of the linearized closed-loop system consisting of (2.2) and (3.35) can be written as

$$(s^2 + bs + c)(s^2 + ds + e). \tag{3.39}$$

The design parameters b and c are associated with the flux observer, and the design parameters d and e are associated with the speed-adaptation loop. Ideally, the poles of the flux observer can be placed independently of the speed adaptation.

3.3 High-Frequency Signal-Injection Methods

The inherently salient structure of synchronous reluctance motors makes it naturally suitable for signal-injection methods. In signal-injection methods, a high-frequency voltage (or current) excitation is superimposed on the back-EMF.

The most common excitation signals are alternating excitation and rotating excitation, while other excitation signals can be used as well. For example, the low-speed position estimation in [Ichikawa et al., 2003] is based on recursive system-parameter identification with M-sequence excitation. Although some authors favour rotating excitation [Jansen and Lorenz, 1995, Consoli et al., 1999, Agarlită et al., 2012], the benefits of this approach compared to alternating excitation have been inconclusive [Raca et al., 2008]. The alternating excitation is less sensitive to inverter dead-time [Raca et al., 2008], while the rotating injection may be advantageous if the motor has multiple saliencies [Degner and Lorenz, 1998].

A simple position-estimation method was introduced in [Consoli et al., 2007], where a high-frequency voltage excitation was superimposed on the stator voltage in the estimated d-axis direction. The magnitude of the high-frequency current response in the q-axis direction was tracked. A minimum-search algorithm was applied to vary the injection direction in such a way that the magnitude of the q-axis high-frequency current would be minimized. This method can be regarded as an improvement of the method proposed in [Consoli et al., 1999], where a rotating voltage injection was used and the position information was determined from the occurrence of the minimum high-frequency current. The speed estimate used in the speed-control loop was obtained from the PI-based mechanism

$$\hat{\omega}_\mathrm{m} = \int k_\mathrm{J} \epsilon \mathrm{d}t \tag{3.40a}$$

$$\epsilon = k_\mathrm{Te} \hat{T}_\mathrm{e} + k_\mathrm{p} \left(\frac{\mathrm{d}\hat{\vartheta}}{\mathrm{d}t} - \hat{\omega}_\mathrm{m} \right) + k_\mathrm{i} \left(\hat{\vartheta} - \int \hat{\omega}_\mathrm{m} \mathrm{d}t \right), \tag{3.40b}$$

where $\hat{\vartheta}$ is the estimated position, $\hat{T}_\mathrm{e}$ is the estimated electromagnetic torque and k_J and k_Te are adaptation gains corresponding to the inertia and electromagnetic torque, respectively.

A high-frequency current excitation was applied in [Kang et al., 1999]. A current excitation of the same magnitude was superimposed on the stator current in both the d- and q-axis direction

$$\boldsymbol{i}_\mathrm{c} = \begin{bmatrix} i_\mathrm{c} \cos(\omega_\mathrm{c} t) \\ i_\mathrm{c} \sin(\omega_\mathrm{c} t) \end{bmatrix}, \tag{3.41}$$

where i_c is the magnitude of the injected current and ω_c is the injection angular frequency. The position-estimation error is extracted from the induced high-frequency voltage responses, which were demodulated and low-pass filtered (LPF)

$$\Delta\hat{\vartheta} \approx \frac{\mathrm{LPF}\left\{ u_\mathrm{cd} \cos(\omega_\mathrm{c} t) - u_\mathrm{cq} \sin(\omega_\mathrm{c} t) \right\}}{(\hat{L}_\mathrm{d} - \hat{L}_\mathrm{q})(\omega_\mathrm{c} + \hat{\omega}_\mathrm{m}) i_\mathrm{c}}, \tag{3.42}$$

where u_cd and u_cq are the d- and q-axis components of the induced high-frequency voltage responses, respectively. The position-estimation error $\Delta\hat{\vartheta}$ is then used to directly update the position estimate. The estimated speed is obtained from the time derivative of the position estimate.

The signal-injection method used in this thesis utilizes alternating high-frequency voltage excitation in the estimated d-axis direction [Corzine et al., 1998],

$$\boldsymbol{u}_\mathrm{c} = \begin{bmatrix} u_\mathrm{c} \cos(\omega_\mathrm{c} t) \\ 0 \end{bmatrix}, \tag{3.43}$$

where u_c is the magnitude of the voltage excitation.

If the rotational speed and the resistive voltage drop are omitted, the high-frequency current responses are

$$i_\mathrm{cd} = \frac{u_\mathrm{c}\sin(\omega_\mathrm{c}t)}{\omega_\mathrm{c}L_\mathrm{det}}\left[L_\Sigma - L_\Delta\cos(2\tilde{\vartheta}_\mathrm{m}) - L_\mathrm{dq}\sin(2\tilde{\vartheta}_\mathrm{m})\right] \tag{3.44a}$$

$$i_\mathrm{cq} = \frac{u_\mathrm{c}\sin(\omega_\mathrm{c}t)}{\omega_\mathrm{c}L_\mathrm{det}}\left[L_\Delta\sin(2\tilde{\vartheta}_\mathrm{m}) - L_\mathrm{dq}\cos(2\tilde{\vartheta}_\mathrm{m})\right], \tag{3.44b}$$

where

$$L_\mathrm{det} = L_\mathrm{dd}L_\mathrm{qq} - L_\mathrm{dq}^2 \tag{3.45a}$$

$$L_\Sigma = \frac{L_\mathrm{dd} + L_\mathrm{qq}}{2} \tag{3.45b}$$

$$L_\Delta = \frac{L_\mathrm{dd} - L_\mathrm{qq}}{2}. \tag{3.45c}$$

The position information is extracted from the current responses via demodulation and low-pass filtering [Harnefors and Nee, 2000, Villet et al., 2012]. Conventionally, only the high-frequency current component perpendicular to the injected signal is used in the position estimation,

$$\begin{aligned}\epsilon &= \mathrm{LPF}\left\{i_\mathrm{q}\sin(\omega_\mathrm{c}t)\right\}\\ &\approx \frac{u_\mathrm{c}}{2\omega_\mathrm{c}L_\mathrm{det}}\left[L_\Delta\sin(2\tilde{\vartheta}_\mathrm{m}) - L_\mathrm{dq}\cos(2\tilde{\vartheta}_\mathrm{m})\right].\end{aligned} \tag{3.46}$$

Usually, signal-injection based position estimation is designed to find a direction where $\epsilon = 0$. Due to cross-saturation, this straightforward scheme (3.46) leads to a steady-state position-estimation error [Guglielmi et al., 2006]

$$\tilde{\vartheta}_\mathrm{m0} = \frac{1}{2}\arctan\left(\frac{L_\mathrm{dq}}{L_\Delta}\right). \tag{3.47}$$

The method proposed in Publication VI to compensate the position-estimation error caused by the cross-saturation is to use a combination of the d- and q-axis current components, which is demodulated and low-pass filtered,

$$\begin{aligned}\epsilon &= \mathrm{LPF}\left\{\left(\frac{\hat{L}_\mathrm{dq}}{\hat{L}_\mathrm{qq}}i_\mathrm{d} + i_\mathrm{q}\right)\sin(\omega_\mathrm{c}t)\right\}\\ &\approx -\frac{u_\mathrm{c}}{2\omega_\mathrm{c}L_\mathrm{det}\hat{L}_\mathrm{qq}}\left(L_\mathrm{dq}\hat{L}_\mathrm{qq} + \hat{L}_\mathrm{dq}L_\Delta\right)\cos(2\tilde{\vartheta}_\mathrm{m})\\ &+ \frac{u_\mathrm{c}}{2\omega_\mathrm{c}L_\mathrm{det}\hat{L}_\mathrm{qq}}\left(L_\Delta\hat{L}_\mathrm{qq} - L_\mathrm{dq}\hat{L}_\mathrm{dq}\right)\sin(2\tilde{\vartheta}_\mathrm{m})\\ &+ \frac{u_\mathrm{c}}{2\omega_\mathrm{c}L_\mathrm{det}\hat{L}_\mathrm{qq}}\left(L_\Delta\hat{L}_\mathrm{dq} + L_\mathrm{qq}\hat{L}_\mathrm{dq}\right).\end{aligned} \tag{3.48}$$

If accurate compensation and small position-estimation error are assumed, the error signal reduces to

$$\epsilon \approx k_\epsilon\sin(2\tilde{\vartheta}_\mathrm{m}), \tag{3.49}$$

where

$$k_\epsilon = \frac{u_\mathrm{c}}{\omega_\mathrm{c}} \frac{L_\Delta \hat{L}_\mathrm{qq} - L_\mathrm{dq} \hat{L}_\mathrm{dq}}{2 L_\mathrm{det} L_\mathrm{qq}} \tag{3.50}$$

is the signal-injection gain. This approach is closely related to the approach used in [Capecchi et al., 2001], where the high-frequency component of the q-axis flux estimate was used in position estimation.

Even with correct compensation for cross-saturation, the signal-injection method (3.43) does not necessarily provide accurate position information at high speeds. For simplicity, the resistive voltage drop in (2.3) is omitted, and it is assumed that the motor does not saturate, i.e. $L_\mathrm{dd} = L_\mathrm{d}$, $L_\mathrm{qq} = L_\mathrm{q}$ and $L_\mathrm{dq} = 0$. The current responses are

$$i_\mathrm{cd} = A_1 \cos(\omega_\mathrm{c} t) + A_2 \sin(\omega_\mathrm{c} t) \tag{3.51a}$$

$$i_\mathrm{cq} = A_3 \cos(\omega_\mathrm{c} t) + A_4 \sin(\omega_\mathrm{c} t), \tag{3.51b}$$

where

$$A_1 = \frac{u_\mathrm{c} \omega_\mathrm{m} L_\Delta \sin(2\tilde{\vartheta}_\mathrm{m})}{L_\mathrm{det}(\omega_\mathrm{c}^2 - \omega_\mathrm{m}^2)} \tag{3.51c}$$

$$A_2 = \frac{u_\mathrm{c} \omega_\mathrm{c} \left[L_\Sigma - L_\Delta \cos(2\tilde{\vartheta}_\mathrm{m}) \right]}{L_\mathrm{det}(\omega_\mathrm{c}^2 - \omega_\mathrm{m}^2)} \tag{3.51d}$$

$$A_3 = \frac{u_\mathrm{c} \omega_\mathrm{m} \left[L_\Sigma + L_\Delta \cos(2\tilde{\vartheta}_\mathrm{m}) \right]}{L_\mathrm{det}(\omega_\mathrm{c}^2 - \omega_\mathrm{m}^2)} \tag{3.51e}$$

$$A_4 = \frac{u_\mathrm{c} \omega_\mathrm{c} L_\Delta \sin(2\tilde{\vartheta}_\mathrm{m})}{L_\mathrm{det}(\omega_\mathrm{c}^2 - \omega_\mathrm{m}^2)}. \tag{3.51f}$$

Due to system delays, the actual current responses (3.51) lag the excitation signal (3.43) by some phase shift ϕ_d, which should be accounted for. When (3.51b) is multiplied by $\sin(\omega_\mathrm{c} t + \phi_\mathrm{d})$ this results in

$$\begin{aligned} i_\mathrm{cq} \sin(\omega_\mathrm{c} t + \phi_\mathrm{d}) = {} & \frac{A_4 \cos(\phi_\mathrm{d}) + A_3 \sin(\phi_\mathrm{d})}{2} \\ & + \frac{A_3 \sin(2\omega_\mathrm{c} t + \phi_\mathrm{d}) - A_4 \cos(2\omega_\mathrm{c} t + \phi_\mathrm{d})}{2}, \end{aligned} \tag{3.52}$$

where the high-frequency components can be omitted due to low-pass filtering. If there is no demodulation error, $i_\mathrm{cq} = 0$ only when $\sin(2\tilde{\vartheta}_\mathrm{m})$.

However, if demodulation error exists, the steady-state position-estimation error is determined by

$$A \cos 2\tilde{\vartheta}_\mathrm{m0} + B \sin 2\tilde{\vartheta}_\mathrm{m0} + C = 0, \tag{3.53a}$$

where

$$A = L_\Delta \omega_\mathrm{m} \sin(\phi_\mathrm{d}) \tag{3.53b}$$

$$B = L_\Delta \omega_\mathrm{c} \cos(\phi_\mathrm{d}) \tag{3.53c}$$

$$C = L_\Sigma \omega_\mathrm{m} \sin(\phi_\mathrm{d}). \tag{3.53d}$$

The solution for the steady-state position-estimation error is obtained in a fashion similar to (3.23). It can be seen that if demodulation error exists, the position-estimation error increases with the speed.

The effect of the demodulation error is illustrated in Figure 3.2 for demodulation delays of 0.5, 1 and 1.5 samples. The motor parameters are $L_\mathrm{d} = 2.0$ p.u. and $L_\mathrm{q} = 0.3$ p.u. The injection frequency is $\omega_\mathrm{c} = 2\pi \cdot 500$ rad/s and the sampling frequency is 5000 Hz. It can be seen that in this case the position-estimation error at the rated speed with system delay of 1.5 samples is nearly 20 degrees.

3.4 Combined Observers

The signal-injection methods can provide reliable position estimate at all speeds from standstill to rated speed. However, the injected high-frequency excitation inflicts the system with additional noise and losses, and they limit the maximum usable voltage. Therefore, several authors have used combined observer, which rely on signal-injection methods only at low speeds. As the speed increases, the amplitude of the injected high-frequency excitation decreases and the underlying back-EMF-based method begins to dominate the position estimation. Finally, the high-frequency excitation is removed when the speed is above the desired transition speed, and the system relies only on the information provided by the back-EMF-based method.

The information provided by the signal injection can be utilized in various ways. In [Ha et al., 1999], a high-frequency current excitation was injected in the estimated d-axis direction. The position information is extracted from the induced high-frequency voltage responses with multiplication and low-pass filtering

$$\epsilon = \mathrm{LPF}\left\{u_\mathrm{cd} u_\mathrm{cq}\right\} \approx \frac{L_\mathrm{d} - L_\mathrm{q}}{2} L_\mathrm{d} \omega_\mathrm{c}^2 i_\mathrm{c}^2 \tilde{\vartheta}_\mathrm{m}. \tag{3.54}$$

This error signal is driven to zero with the PI-mechanism

$$\hat{\omega}_\mathrm{m} = k_\mathrm{p}\epsilon + \int k_\mathrm{i}\epsilon \mathrm{d}t, \tag{3.55}$$

from which the position information is obtained according to (3.21). The overall position estimate is a weighted sum of this and the position estimate obtained from (3.5), with weight on the signal-injection method at low speeds.

The high-frequency current excitation was also used in [Kato et al., 2011]. At high speeds, the position estimation is based on the method

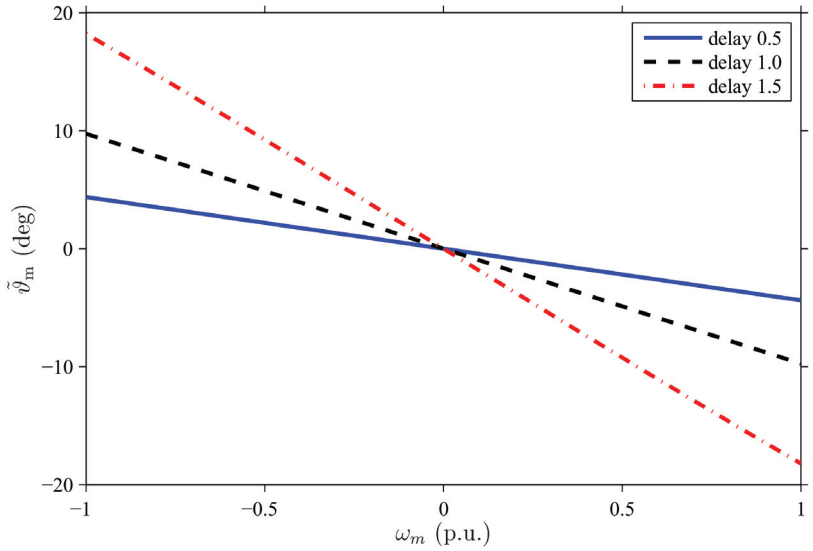

Figure 3.2. Position-estimation error caused by demodulation delay in signal injection, with different delays as function of speed: 0.5 samples (solid line), 1 sample (dashed line), and 1.5 samples (dashed-dotted line). The injection frequency is 500 Hz, and the sampling frequency is 5000 Hz.

presented in [Ichikawa et al., 2003], but near standstill the position information is extracted via disturbing the EEMF (3.11) with a high-frequency current injection. The high-frequency components of the EEMF are estimated using a reduced-order observer, and the position information is extracted from the EEMF as in (3.12).

In [Capecchi et al., 2001], a high-frequency excitation is superimposed on the d-axis flux reference. The high-frequency component of the q-axis flux estimate is driven to zero in a fashion similar to (3.55). This speed estimate is then combined with the speed estimate from the back-EMF model (3.10).

A rotating voltage excitation in the stator-reference frame was used in [Agarlită et al., 2012]. After demodulation and low-pass filtering, the position information is extracted from the negative-sequence current response, utilizing a phase-locked loop based on the work presented in [Lorenz and Patten, 1991]. The overall position estimate is a weighted sum of the position estimate provided by the back-EMF method and the high-frequency method, with the weight moving to the back-EMF as the speed increases.

The method proposed in [Piippo et al., 2004] utilizes the error signal ϵ

(3.46) directly in both the speed and position estimation,

$$\hat{\omega}_\mathrm{m} = \frac{\hat{e}_\mathrm{q}}{\hat{\psi}_\mathrm{pm}} + \gamma_\mathrm{i} \int \epsilon \mathrm{d}t \tag{3.56a}$$

$$\hat{\vartheta}_\mathrm{m} = \int (\hat{\omega}_\mathrm{m} + \gamma_\mathrm{p}\epsilon)\,\mathrm{d}t, \tag{3.56b}$$

where γ_p and γ_i are adaptation gains, $\hat{e}_\mathrm{q}$ is the q-axis component of the back-EMF and $\hat{\psi}_\mathrm{pm}$ is the magnitude of the estimated permanent-magnet flux. When the signal injection is not used, the speed estimation is based on the pure voltage model.

In the combined observer proposed in [Piippo and Luomi, 2005] and used in Publication VI, the error signal ϵ is driven to zero using the PI-mechanism

$$\omega_\epsilon = \gamma_\mathrm{p}\epsilon + \gamma_\mathrm{i} \int \epsilon \mathrm{d}t. \tag{3.57}$$

The adaptation gains are

$$\gamma_\mathrm{p} = \frac{\alpha_\mathrm{i}}{2k_\epsilon}, \quad \gamma_\mathrm{i} = \frac{\alpha_\mathrm{i}^2}{6k_\epsilon}, \tag{3.58}$$

where α_i is the approximate bandwidth of the PI mechanism, k_ϵ is the signal-injection gain (3.50) and the bandwidth of the low-pass filter in (3.46) or (3.48) is $\alpha_\mathrm{lp} = 3\alpha_\mathrm{i}$. The speed correction term ω_ϵ is then incorporated in the flux observer (3.35a) according to

$$\frac{\mathrm{d}\hat{\boldsymbol{\psi}}_\mathrm{s}}{\mathrm{d}t} = \boldsymbol{u}_\mathrm{s} - \hat{R}_\mathrm{s}\hat{\boldsymbol{i}}_\mathrm{s} - (\hat{\omega}_\mathrm{m} + \omega_\epsilon)\mathbf{J}\hat{\boldsymbol{\psi}}_\mathrm{s} + \boldsymbol{K}\tilde{\boldsymbol{i}}_\mathrm{s}. \tag{3.59}$$

The gain selection (3.58) was derived in [Piippo and Luomi, 2005], assuming fast flux-tracking loop and slow speed-tracking loop. If the situation is reversed, the gain selection has to be modified. Assuming accurate model parameter estimates and the speed-adaptation law (3.35d) in the steady state, i.e. $\tilde{i}_\mathrm{q} = 0$, the characteristic polynomial of the linearized closed-loop system consisting of (2.2), (3.35c), (3.49), (3.57), and (3.59) is

$$s^4 + A_3 s^3 + A_2 s^2 + A_1 s + A_0, \tag{3.60a}$$

where

$$A_3 = \alpha_\mathrm{lp} - k_{11} + \beta k_{21} \tag{3.60b}$$

$$A_2 = \frac{2k_\epsilon}{L_\mathrm{d} - L_\mathrm{q}} \alpha_\mathrm{lp} L_\mathrm{d} \gamma_\mathrm{p} - \alpha_\mathrm{lp}(k_{11} - \beta k_{21}) - \hat{\omega}_\mathrm{m}(k_{21} - \hat{\omega}_\mathrm{m} + \beta k_{11}) \tag{3.60c}$$

$$A_1 = \frac{2k_\epsilon}{L_\mathrm{d} - L_\mathrm{q}} \alpha_\mathrm{lp} \left[L_\mathrm{d}(\gamma_\mathrm{i} - \gamma_\mathrm{p} k_{11}) + L_\mathrm{q}\beta\gamma_\mathrm{p}(\hat{\omega}_\mathrm{m} - k_{21})\right] - \alpha_\mathrm{lp}\hat{\omega}_\mathrm{m}(k_{21} - \hat{\omega}_\mathrm{m} + \beta k_{11}) \tag{3.60d}$$

$$A_0 = \frac{2k_\epsilon}{L_\mathrm{d} - L_\mathrm{q}} \alpha_\mathrm{lp} \gamma_\mathrm{i} (L_\mathrm{q}\beta(\hat{\omega}_\mathrm{m} - k_{21}) - L_\mathrm{d} k_{11}) \tag{3.60e}$$

and α_{lp} is the bandwidth of the low-pass filter in (3.48).

For design purposes, the characteristic polynomial is written as

$$(s^2 + bs + c)(s + \alpha'_{\mathrm{lp}})(s + \alpha_\epsilon), \tag{3.61}$$

where b and c are design parameters associated with the flux observer, and α'_{lp} and α_ϵ are design parameters associated with the low-pass filter (3.48) and the speed-correction loop (3.57), respectively. Equating (3.60) and (3.61), the gains of the augmented observer can be written as functions of the design parameters $\{b, c, \alpha'_{\mathrm{lp}}, \alpha_\epsilon\}$, which all should be positive in order to stabilize the system. Other design parameter sets could be chosen as well.

When b, c, α'_{lp}, and α_ϵ are the design parameters, the observer gain k_{11} is determined by

$$k_{11} = \beta k_{21} - b - \alpha_\epsilon + \alpha_{\mathrm{lp}} - \alpha'_{\mathrm{lp}} \tag{3.62a}$$

and the PI gains γ_{i} and γ_{p} are

$$\gamma_{\mathrm{i}} = \frac{L_{\mathrm{d}} - L_{\mathrm{q}}}{2k_\epsilon} \frac{\alpha'_{\mathrm{lp}} \alpha_\epsilon c}{\alpha_{\mathrm{lp}} \left[L_{\mathrm{q}} \beta (\hat{\omega}_{\mathrm{m}} - k_{21}) - L_{\mathrm{d}} k_{11} \right]} \tag{3.62b}$$

$$\begin{aligned} \gamma_{\mathrm{p}} = {} & \frac{L_{\mathrm{d}} - L_{\mathrm{q}}}{2k_\epsilon} \frac{\hat{\omega}_{\mathrm{m}}(k_{21} - \hat{\omega}_{\mathrm{m}} + \beta k_{11})}{L_{\mathrm{q}} \beta (\hat{\omega}_{\mathrm{m}} - k_{21}) - L_{\mathrm{d}} k_{11}} \\ & + \frac{L_{\mathrm{d}} - L_{\mathrm{q}}}{2k_\epsilon} \frac{\alpha'_{\mathrm{lp}}(c + b\alpha_\epsilon) + c\alpha_\epsilon}{\alpha_{\mathrm{lp}} \left[L_{\mathrm{q}} \beta (\hat{\omega}_{\mathrm{m}} - k_{21}) - L_{\mathrm{d}} k_{11} \right]} \\ & - \frac{L_{\mathrm{d}} \gamma_{\mathrm{i}}}{L_{\mathrm{q}} \beta (\hat{\omega}_{\mathrm{m}} - k_{21}) - L_{\mathrm{d}} k_{11}}. \end{aligned} \tag{3.62c}$$

The remaining constraint from (3.60) and (3.61) is a cubic equation for α'_{lp}. However, if sufficiently large bandwidth is selected for the low-pass filter, then $\alpha'_{\mathrm{lp}} = \alpha_{\mathrm{lp}}$ can be approximated, as is done in Publication VII.

Since the parameter uncertainties are compensated for by ω_ϵ in (3.59), the behaviour of ω_ϵ at low speeds should be considered. It can be shown from (2.2), (3.35c) and (3.59) that when $\hat{\omega}_{\mathrm{m}} = 0$, the steady-state solution for ω_ϵ is obtained from

$$\beta \hat{L}_{\mathrm{q}} \omega_\epsilon^2 - (\tilde{R}_{\mathrm{s}} + \hat{L}_{\mathrm{d}} k_1 + \hat{L}_{\mathrm{q}} \beta k_2) \omega_\epsilon + \tilde{R}_{\mathrm{s}} (k_2 - \beta k_1) = 0. \tag{3.63}$$

Depending on the parameter estimates and gain selection, real valued (stabilizing) solutions for (3.63) might not exist. Moreover, in [Piippo and Luomi, 2005] it was suggested that ω_ϵ should be limited between some small values $-\omega_{\epsilon,\mathrm{lim}}$ and $\omega_{\epsilon,\mathrm{lim}}$. Even if the solutions for (3.63) are real valued, it is not easy to assure that both solutions are small, and ω_ϵ might reach the limit with no practical contribution to the position correction. Hence, the combined observer (3.59) might easily become unstable when

applied for synchronous reluctance motor drives if the gain selection is not carefully inspected with even small parameter uncertainties. Due to these problems, an alternative method to utilize the error signal ϵ was proposed in Publication VII.

4. Parameter Adaptation

The accuracy and stability of the back-EMF-based methods considered in this thesis depend on the parameters of the equivalent-circuit model. However, only a few works have addressed practical approaches to obtain the model parameters without preliminary measurements for position-sensorless synchronous reluctance motor drives.

Methods based on recursive system parameter identification were used in [Ghaderi et al., 2006] and [Ichikawa et al., 2006], where [Ghaderi et al., 2006] utilizes block-pulse function excitation and [Ichikawa et al., 2006] utilizes M-sequence excitation. A simple method to estimate the average inductance was proposed in [Paulus et al., 2011]. The method was intended to be used with the observer proposed in [Stumper et al., 2010]. However, it was assumed in the derivation that $i_\mathrm{d} = i_\mathrm{q}$, which is not always the case.

In order to avoid preliminary measurements requiring additional hardware, methods to estimate the motor model parameters during normal operation of the drive were proposed in Publication II and Publication VII. The overall observer structure is illustrated in Figure 4.1.

4.1 Stator-Resistance Adaptation Using Fundamental Excitation

For improved low-speed operation, the reduced-order observer (3.27) can be augmented with the stator-resistance adaptation law

$$\hat{R}_\mathrm{s} = \int k_\mathrm{R} \hat{L}_\mathrm{d} \tilde{i}_\mathrm{d} \mathrm{d}t. \tag{4.1}$$

Since in this method the d-axis current-estimation error is driven to zero, the steady-state estimation errors are independent of the gain selections. The steady-state resistance-estimation error derived in Publication IV is

$$\tilde{R}_\mathrm{s0} = \hat{\omega}_\mathrm{m}(L_\mathrm{d} - L_\mathrm{q}) \frac{\cos(2\tilde{\vartheta}_\mathrm{m0}) - \beta \sin(2\tilde{\vartheta}_\mathrm{m0}) - 1}{2\beta} - \frac{\hat{\omega}_\mathrm{m}}{\beta} \tilde{L}_\mathrm{d}. \tag{4.2}$$

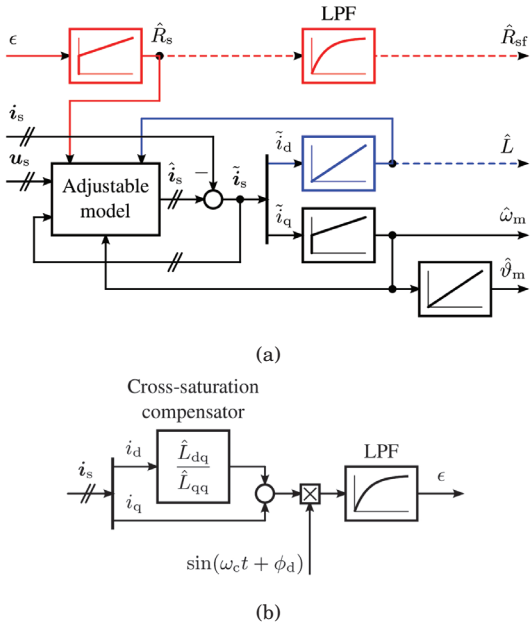

Figure 4.1. (a) Adaptive observer. The adjustable model is defined in (3.35). The blue lines and blocks represent inductance adaptation, and the red lines and blocks represent resistance adaptation. (b) Error-signal calculation scheme. The bandwidth of the first-order low-pass filter (LPF) is α_lp. The effect of the discretization delay on the demodulation process is compensated for by means of the constant parameter ϕ_d.

It can be seen that $\tilde{R}_\mathrm{s0}$ increases as the speed increases or β decreases, suggesting that the stator-resistance adaptation should be used only at low speeds and high load. Since the resistance estimation is based on eliminating the d-axis flux-estimation error $\tilde{\psi}_\mathrm{d}$ in the steady state, this method is strongly dependent on the accuracy of $\hat{L}_\mathrm{d}$. The properties and tuning of the stator-resistance adaptation are discussed in more detail in Publication II and Publication IV.

4.2 Inductance-Adaptation Using Fundamental Excitation

The approach to adjust the inductance estimates is to use the adaptation law

$$\hat{L} = \int k_\mathrm{L} \hat{L}_\mathrm{d} \tilde{i}_\mathrm{d} \mathrm{d}t, \tag{4.3}$$

where only the current-estimation error in the d-axis direction is used. Since the speed-adaptation loop drives $\tilde{i}_\mathrm{q}$ to zero and the inductance-adaptation loop drives $\tilde{i}_\mathrm{d}$ to zero, all the steady-state estimation errors are independent of the gain selections. The method is closely related to the

permanent-magnet flux adaptation law proposed in [Piippo et al., 2009].

The same adaptation law (4.3) can be used for both the d-axis inductance and the q-axis inductance. The resulting steady-state inductance estimates, derived in Publication VI, are

$$\hat{L}_\mathrm{d} = \frac{L_\mathrm{d}+L_\mathrm{q}}{2} - \frac{\beta\tilde{R}_\mathrm{s}}{\hat{\omega}_\mathrm{m}} + \frac{L_\mathrm{d}-L_\mathrm{q}}{2}\cos(2\tilde{\vartheta}_\mathrm{m0}) - \beta\frac{L_\mathrm{d}-L_\mathrm{q}}{2}\sin(2\tilde{\vartheta}_\mathrm{m0}) \quad \text{(4.4a)}$$

$$\hat{L}_\mathrm{q} = \frac{L_\mathrm{d}+L_\mathrm{q}}{2} + \frac{\tilde{R}_\mathrm{s}}{\beta\hat{\omega}_\mathrm{m}} - \frac{L_\mathrm{d}-L_\mathrm{q}}{2}\cos(2\tilde{\vartheta}_\mathrm{m0}) - \frac{L_\mathrm{d}-L_\mathrm{q}}{2\beta}\sin(2\tilde{\vartheta}_\mathrm{m0}). \quad \text{(4.4b)}$$

Both inductance estimates are inversely proportional to the speed, which suggests that the inductances should be adapted only at high speeds. On the other hand, $\hat{L}_\mathrm{d}$ is proportional to β and $\hat{L}_\mathrm{q}$ is inversely proportional to β, which suggests that $\hat{L}_\mathrm{d}$ should be adapted at low loads and $\hat{L}_\mathrm{q}$ should be adapted at high loads. The properties and tuning of the inductance adaptation are discussed in more detail in Publication VII.

4.3 Stator-Resistance Adaptation Using High-Frequency Signal Injection

The stator-resistance adaptation mechanism proposed in [Piippo et al., 2009] utilized an integrator to drive the speed-correction term ω_ϵ (3.57) to zero. The overall combined observer with the signal injection and the resistance adaptation is of the seventh order.

The method proposed in Publication VII is to combine the information provided by the signal injection with the flux observer via updating the stator-resistance estimate directly without intermediate states,

$$\hat{R}_\mathrm{s} = \gamma_\mathrm{p}\epsilon + \int \gamma_\mathrm{i}\epsilon \mathrm{d}t. \quad \text{(4.5)}$$

The additional integrator can be removed, and the order of the overall system is reduced by one.

Since the signal injection does not affect the steady-state error equation, $\tilde{R}_\mathrm{s}$ can be solved from (3.29) as function of the position-estimation error, inductance errors and observer gains,

$$\begin{aligned}\tilde{R}_\mathrm{s} =& \hat{\omega}_\mathrm{m}\frac{L_\mathrm{d}-L_\mathrm{q}}{2}\frac{k_{11}-\beta k_{21}+\beta\hat{\omega}_\mathrm{m}}{\hat{\omega}_\mathrm{m}-k_{21}+\beta k_{11}}\left[1-\cos(2\tilde{\vartheta}_\mathrm{m0})\right] \\ &+ \hat{\omega}_\mathrm{m}\frac{L_\mathrm{d}-L_\mathrm{q}}{2}\frac{k_{21}-\hat{\omega}_\mathrm{m}+\beta k_{11}}{k_{21}-\hat{\omega}_\mathrm{m}-\beta k_{11}}\sin(2\tilde{\vartheta}_\mathrm{m0}) \\ &+ \hat{\omega}_\mathrm{m}\frac{\tilde{L}_\mathrm{d}k_{11}+\tilde{L}_\mathrm{q}\beta(k_{21}-\hat{\omega}_\mathrm{m})}{k_{21}-\hat{\omega}_\mathrm{m}-\beta k_{11}},\end{aligned} \quad \text{(4.6)}$$

where k_1 and k_2 have been replaced with k_{11} and k_{21}, respectively. It can be seen that at standstill the estimation error is zero regardless of

the position-estimation error. In no-load condition, if $\tilde{\vartheta}_{\mathrm{m}0} = 0$ is obtained, the resistance-estimation error increases proportionally to $\hat{\omega}_{\mathrm{m}}\tilde{L}_{\mathrm{d}}k_{11}/(k_{21} - \hat{\omega}_{\mathrm{m}})$. This behaviour should be considered in more detail, if accurate resistance estimate is desired at low speeds. The properties and tuning of the resistance adaptation are discussed in more detail in Publication VII.

5. Summaries of Publications

5.1 Abstracts

Publication I

This paper deals with reduced-order observers with stator-resistance adaptation for motion-sensorless permanent-magnet synchronous motor drives. An analytical solution for the stabilizing observer gain and stability conditions for the stator-resistance adaptation are derived. The proposed observer design is experimentally tested using a 2.2-kW motor drive; stable operation at very low speeds under different loading conditions is demonstrated.

Publication II

A reduced-order position observer with stator-resistance adaptation is applied for motion-sensorless synchronous reluctance motor drives. A general analytical solution for the stabilizing observer gain and stability conditions for the stator-resistance adaptation are given. The local stability of the position and stator-resistance estimation is guaranteed at every operating point except the zero frequency, if inductances are known accurately. The observer design is experimentally tested using a 6.7-kW synchronous reluctance motor drive; stable operation at low speeds under various loading conditions is demonstrated.

Publication III

This paper deals with the modeling of the magnetic saturation in synchronous reluctance motors (SyRMs). The saturation is modeled by

means of analytical expressions, which can be easily embedded in dynamic equivalent-circuit models. A modified power function - proposed in this paper - can take into account the cross saturation between the orthogonal windings, it is physically consistent, and the number of its parameters is small. The function can be used in real-time control applications and in computer simulations. The model fits well to the experimentally measured inductances of a 6.7-kW SyRM. As an application example, the proposed saturation model was implemented in a full-order observer of a motion-sensorless drive, and experimental results are shown.

Publication IV

A back-electromotive-force-based reduced-order position observer with stator-resistance adaptation is analyzed for motion-sensorless synchronous reluctance motor (SyRM) drives. Analytical equations for steady-state estimation errors and stability conditions are derived (with and without resistance adaptation), taking into account errors in the parameter estimates. The effect of the observer gain on the noise reduction is studied by means of eigenvector analysis. A robust gain selection is proposed, which maximizes the allowed uncertainties in the parameter estimates. The proposed observer design is experimentally evaluated using a 6.7-kW SyRM drive; stable operation is demonstrated at low speeds under various parameter errors.

Publication V

Two back-electromotive-force-based position observers are compared for motion-sensorless synchronous motor drives: the reduced-order observer and the adaptive full-order observer. A stabilizing gain is proposed for the adaptive full-order observer, which guarantees the local stability of the closed-loop system, if the motor parameters are known. Equations for the steady-state position error and for the linearized estimation-error dynamics under erroneous parameters are derived, and the robustness of the two observers against parameter errors is analyzed and compared. The observers are experimentally evaluated using a 6.7-kW synchronous reluctance motor drive in low-speed operation and under parameter errors. The gain selection of the reduced-order observer is easier, but the adaptive full-order observer can be made more robust against parameter variations and noise.

Publication VI

A back-EMF-based position observer for motion-sensorless synchronous reluctance motor drives is augmented with high-frequency signal-injection method for improved lowspeed operation. Previously proposed observer structure is further improved to account for the cross saturation in the motor. The combined observer is experimentally evaluated using a 6.7- kW synchronous reluctance motor drive in low-speed operation and under various load conditions. The resulting position error at low speeds and standstill is small.

Publication VII

A back-EMF-based position observer for motion-sensorless synchronous reluctance motor (SyRM) drives is augmented with parameter-adaptation laws for improved operation at all speeds, including standstill. The augmented observer is theoretically analyzed under various operation conditions. The analysis indicates that the stator-resistance adaptation should be enabled only at low speeds, the d-axis inductance adaptation should be enabled only at medium and high speeds near no load, and the q-axis inductance adaptation should be enabled only at high speeds under high load. The augmented observer is experimentally evaluated using a 6.7-kW SyRM drive.

5.2 Contribution of the Thesis

The main contributions of the thesis can be summarized as follows:

- Saturation models for synchronous reluctance motors were compared, and a physically reasonable saturation model for synchronous reluctance motors was proposed. (Publication III)

- Steady-state position-estimation error and stability of a simple first-order observer were analyzed under erroneous model parameters. (Publication I, Chapter 3)

- Steady-state estimation errors and stability of a reduced-order observer were analyzed under erroneous model parameters. Based on the anal-

ysis, robust gain selection was proposed with maximal tolerance for model parameter uncertainties. (Publication IV)

- The reduced-order observer was augmented with resistance-adaptation mechanism for improved low-speed operation. The steady-state estimation error and stability of the resistance adaptation were analyzed under erroneous model parameters. Based on the analysis, stabilizing gain selection for the augmented observer was proposed. (Publication II, Publication IV)

- Steady-state estimation errors and stability of a speed-adaptive full-order observer were analyzed under erroneous parameter estimates. Based on the analysis, stabilizing gain selection was proposed. (Publication V)

- Parameter sensitivity and estimation performance of the reduced-order observer and the speed-adaptive full-order observer were compared. (Publication V)

- Compensation mechanism for the position-estimation error caused by cross-saturation in signal-injection assisted full-order observer was proposed. (Publication VI)

- Stabilizing gain selection for the speed-adaptive full-order observer with speed correction from signal injection was proposed. (Publication VI, Chapter 3)

- Inductance-adaptation law using the back-electromotive force was proposed for the speed-adaptive full-order observer. Steady-state estimation errors and stability of the inductance adaptation were analyzed with erroneous model parameters. Based on the analysis, stabilizing gain selection was proposed. (Publication VII)

- Resistance-adaptation law using high-frequency signal injection was proposed for the speed-adaptive full-order observer. Steady-state estimation errors and stability of the resistance adaptation were analyzed with erroneous model parameters. Based on the analysis, stabilizing gain selection was proposed. (Publication VII)

6. Conclusions

Modern synchronous reluctance motors have emerged as feasible competitors to induction motors in variable-speed drives, due to simpler structure and smaller energy losses. In order to operate synchronous reluctance motors, information on the rotor position is needed. In low-cost drives, position-sensorless control methods are often preferred, since the mechanical position encoders are expensive. Moreover, the mechanical encoders are prone to failures, and cannot be installed in certain conditions.

In this thesis, model-based position-estimation methods have been studied for synchronous reluctance motor drives. Since the accuracy of the position estimation depends on the accuracy of the equivalent-circuit model parameters, effects of uncertainties in these model parameters have been analyzed.

The back-electromotive force induced by the rotational movement of the rotor can provide satisfactory position information in order to obtain stable operation at speeds above approximately 5–10% of the rated speed. At lower speeds, modeling errors and measurement noise impair performance, leading possibly to instabilities.

Additional information on the rotor position can be obtained if the drive is excited with additional test signals. The purpose of these test signals is to map the spatial structure of the motor. However, the test signals inflict the system with acoustic noise and increase losses. Furthermore, since the test signals are usually generated by the same frequency converter which supplies the motor with the back-electromotive force, the voltage available for the back-electromotive force is limited when additional test signals are used. Therefore, additional test signals should be used only at the lowest speeds.

Two slightly different ways of combining the information provided by the signal injection with the underlying model based on the back-

electromotive force were considered in Publication VI and Publication VII. The approach used in Publication VI introduces an additional state to the system. This state is then bound in order to limit the corrective effects of the signal injection and in order to decouple the signal injection from the underlying model at high speeds. However, it is not straightforward to determine how the limits should be set. The approach proposed in Publication VII utilizes the information provided by the signal injection directly to update the resistance estimate, but on the other hand, this approach leads to an erroneous resistance estimate as the speed increases, which might impair the performance of the drive in transient states at low speeds.

If the equivalent-circuit model parameters are known in advance with moderate accuracy, the observer gains can be determined following the design guidelines given in Publication IV and Publication V. If the parameters are unknown, or the accuracy is not satisfactory, the parameter adaptation methods proposed in Publication VII can be used. Accurate parameter estimates can be achieved if the results on the estimation accuracy at different operating points are considered. The inductance-adaptation mechanism can be used in an initialization test to obtain the inductances at desired operating points or to obtain saturation-model parameters.

Although several approaches can be used in combining the information provided by the signal injection with the information from the back-electromotive force, no thorough comparison on the benefits and drawbacks of these approaches yet exists. Further, the cross-coupling between the d- and q-axis distorts the position information seen by the signal injection, if the coupling is not compensated for. The compensation method proposed in Publication VI utilized a compensation factor, which was obtained via measuring the incremental inductances with the actual rotor position available. A mechanism to identify the compensation factor without position sensor is still needed.

Bibliography

[Agarlită et al., 2012] Agarlită, S.-C., Boldea, I., and Blaabjerg, F. (2012). High-frequency-injection-assisted "active flux"-based sensorless vector control of reluctance synchronous motors, with experiments from zero speed. *IEEE Trans. Ind. Appl.*, 48(6):1931–1939.

[Arefeen et al., 1994] Arefeen, M. S., Ehsani, M., and Lipo, T. A. (1994). Sensorless position measurement in synchronous reluctance motor. *IEEE Trans. Power Electron.*, 9(6):624–630.

[Boglietti and Pastorelli, 2008] Boglietti, A. and Pastorelli, M. (2008). Induction and synchronous reluctance motors comparison. In *Proc. IEEE IECON'08*, pages 2041–2044, Orlando, FL.

[Capecchi et al., 2001] Capecchi, E., Guglielmo, P., Pastorelli, M., and Vagati, A. (2001). Position-sensorless control of the transverse-laminated synchronous reluctance motor. *IEEE Trans. Ind. Appl.*, 37(6):1768–1776.

[Chen et al., 2004] Chen, C.-G., Liu, T.-H., Lin, M.-T., and Tai, C.-A. (2004). Position control of a sensorless synchronous reluctance motor drive. *IEEE Trans. Ind. Electron.*, 51(1):15–25.

[Choi and Sul, 1996] Choi, J. and Sul, S. (1996). Inverter output voltage synthesis using novel dead time compensation. *IEEE Trans. Power Electron.*, 11(2):221–227.

[Consoli et al., 1999] Consoli, A., Russo, F., Scarcella, G., and Testa, A. (1999). Low- and zero-speed sensorless control of synchronous reluctance motors. *IEEE Trans. Ind. Appl.*, 35(5):1050–1057.

[Consoli et al., 2007] Consoli, A., Scarcella, G., Scelba, G., Testa, A., and Triolo, D. A. (2007). Sensorless rotor position estimation in synchronous reluctance motors exploiting a flux deviation approach. *IEEE Trans. Ind. Appl.*, 43(5):1266–1273.

[Corzine et al., 1998] Corzine, K. A., Kuhn, B. T., Sudhoff, S. D., and Hegner, H. J. (1998). An improved method for incorporating magnetic saturation in the q-d synchronous machine model. *IEEE Trans. Energy Convers.*, 13(3):270–275.

[Cruickshank et al., 1971] Cruickshank, A. J. O., Anderson, A. F., and Menzies, R. W. (1971). Theory and performance of reluctance motors with axially laminated anisotropic rotors. *Proc. IEE*, 118(7):887–894.

[de Kock et al., 2007] de Kock, H. W., Kamper, M. J., Ferreira, O. C., and Kennel, R. M. (2007). Position sensorless control of the reluctance synchronous machine considering high frequency inductances. In *Proc. PEDS 2007*, pages 812–821, Bangkok, Thailand.

[Degner and Lorenz, 1998] Degner, M. W. and Lorenz, R. D. (1998). Using multiple saliencies for the estimation of flux, position, and velocity in AC machines. *IEEE Trans. Ind. Appl.*, 34(5):1097–1104.

[Ghaderi and Hanamoto, 2011] Ghaderi, A. and Hanamoto, T. (2011). Wide-speed-range sensorless vector control of synchronous reluctance motors based on extended programmable cascaded low-pass filters. *IEEE Trans. Ind. Electron.*, 58(6):2322–2333.

[Ghaderi et al., 2006] Ghaderi, A., Hanamoto, T., and Teruo, T. (2006). A novel implementation of low speed sensorless vector control of synchronous reluctance motors with a new online parameter identification approach. In *Proc. IEEE APEC'06*, pages 211–217, Dallas, TX.

[Guglielmi et al., 2006] Guglielmi, P., Pastorelli, M., and Vagati, A. (2006). Impact of cross-saturation in sensorless control of transverse-laminated synchronous reluctance motors. *IEEE Trans. Ind. Electron.*, 53(2):429–439.

[Ha et al., 1999] Ha, J.-I., Kang, S.-J., and Sul, S.-K. (1999). Position-controlled synchronous reluctance motor without rotational transducer. *IEEE Trans. Ind. Appl.*, 35(6):1393–1398.

[Harnefors and Nee, 2000] Harnefors, L. and Nee, H.-P. (2000). A general algorithm for speed and position estimation of AC motors. *IEEE Trans. Ind. Electron.*, 47(1):77–83.

[Ichikawa et al., 2003] Ichikawa, S., Tomita, M., Doki, S., and Okuma, S. (2003). Sensorless control of synchronous reluctance motors based on an extended EMF model and initial position estimation. In *Proc. IEEE IECON'03*, volume 3, pages 2150–2155, Roanoke, VA.

[Ichikawa et al., 2006] Ichikawa, S., Tomita, M., Doki, S., and Okuma, S. (2006). Sensorless control of synchronous reluctance motors based on extended EMF models considering magnetic saturation with online parameter identification. *IEEE Trans. Ind. Appl.*, 42(5):1264–1274.

[Inoue et al., 2010] Inoue, Y., Morimoto, S., and Sanada, M. (2010). A novel control scheme for wide speed range operation of direct torque controlled synchronous reluctance motor. In *Proc. IEEE ECCE'10*, volume 1, pages 192–198, Atlanta, GA.

[Jansen and Lorenz, 1995] Jansen, P. L. and Lorenz, R. D. (1995). Transducerless position and velocity estimation in induction and salient AC machines. *IEEE Trans. Ind. Appl.*, 31(2):240–247.

[Jovanović et al., 1998] Jovanović, M. G., Betz, R. E., and Platt, D. (1998). Sensorless vector controller for a synchronous reluctance motor. *IEEE Trans. Ind. Appl.*, 34(2):346–354.

[Kang et al., 1999] Kang, S.-J., Kim, J.-M., and Sul, S.-K. (1999). Position sensorless control of synchronous reluctance motor using high frequency current injection. *IEEE Trans. Energy Convers.*, 14(4):1271–1275.

[Kato et al., 2011] Kato, K., Tomita, M., Hasegawa, M., Doki, S., Okuma, S., and Kato, S. (2011). Position and velocity sensorless control of synchronous reluctance motor at low speed using disturbance observer for high-frequency extended EMF. In *Proc. IEEE IECON'11*, volume 1, pages 1971–1976, Melbourne, VIC.

[Kostko, 1923] Kostko, J. K. (1923). Polyphase reaction synchronous motors. *Journal of AIEE*, 42(11):1162–1168.

[Kreindler et al., 1993] Kreindler, L., Testa, A., and Lipo, T. (1993). Position sensorless synchronous reluctance motor drive using the stator phase voltage third harmonic. In *Conf. Rec. IEEE-IAS Annu. Meeting*, volume 1, pages 679–686, Toronto, ON.

[Lagerquist et al., 1994] Lagerquist, R., Boldea, I., and Miller, J. (1994). Sensorless control of the synchronous reluctance motor. *IEEE Trans. Ind. Appl.*, 30(3):673–682.

[Landsmann et al., 2010a] Landsmann, P., D.Paulus, Stolze, P., and Kennel, R. (2010a). Saliency based encoderless predictive torque control without signal injection for a reluctance synchronous machine. In *Proc. EPE-PEMC'10*, Ohrid, Macedonia.

[Landsmann et al., 2010b] Landsmann, P., Kennel, R., de Kock, H., and Kamper, M. (2010b). Fundamental saliency based encoderless control for reluctance synchronous machines. In *Proc. ICEM'10*, Rome, Italy.

[Lipo and Krause, 1967] Lipo, T. A. and Krause, P. C. (1967). Stability analysis of a reluctance-synchronous machine. *IEEE Trans. Power App. Syst.*, PAS-86(7):825–834.

[Lorenz, 2001] Lorenz, R. D. (2001). Practical issues and research opportunities when implementing zero speed sensorless control. In *Proc. ICEMS'01*, volume 1, Shenyang, China.

[Lorenz and Patten, 1991] Lorenz, R. D. and Patten, K. W. V. (1991). High-resolution velocity estimation for all-digital, AC servo drives. *IEEE Trans. Ind. Appl.*, 27(4):701–705.

[Matsuo and Lipo, 1995] Matsuo, T. and Lipo, T. A. (1995). Rotor position detection scheme for synchronous reluctance motor based on current measurements. *IEEE Trans. Ind. Appl.*, 31(4):860–868.

[Morales-Caporal and Pacas, 2008] Morales-Caporal, R. and Pacas, M. (2008). Encoderless predictive direct torque control for synchronous reluctance machines at very low and zero speed. *IEEE Trans. Ind. Electron.*, 55(12):4408–4416.

[Paulus et al., 2011] Paulus, D., Stumper, J.-F., Landsmann, P., and Kennel, R. (2011). Encoderless field-oriented control of a synchronous reluctance machine with position and inductance estimators. In *ICPE 2011-ECCE Asia*, pages 1153–1160, Jeju, Korea.

[Pedersen et al., 1993] Pedersen, J. K., Blaabjerg, F., Jensen, J. W., and Thogersen, P. (1993). An ideal PWM-VSI inverter with feedforward and feedback compensation. In *Proc. EPE'93*, volume 4, pages 312–318, Brighton, U.K.

[Piippo et al., 2004] Piippo, A., Hinkkanen, M., and Luomi, J. (2004). Sensorless control of PMSM drives using a combination of voltage model and HF signal injection. In *Conf. Rec. IEEE-IAS Annu. Meeting*, volume 2, pages 964–970, Seattle, WA.

[Piippo et al., 2009] Piippo, A., Hinkkanen, M., and Luomi, J. (2009). Adaptation of motor parameters in sensorless PMSM drives. *IEEE Trans. Ind. Appl.*, 45(1):203–212.

[Piippo and Luomi, 2005] Piippo, A. and Luomi, J. (2005). Adaptive observer combined with HF signal injection for sensorless control of PMSM drives. In *Proc. IEEE IEMDC'05*, pages 674–681, San Antonio, TX.

[Raca et al., 2008] Raca, D., García, P., Reigosa, D., Briz, F., and Lorenz, R. (2008). A comparative analysis of pulsating vs. rotating vector carrier signal injection-based sensorless control. In *Proc. IEEE APEC'08*, pages 879–885, Austin, TX.

[Schroedl and Weinmeier, 1994] Schroedl, M. and Weinmeier, P. (1994). Sensorless control of reluctance machines at arbitrary operating conditions including standstill. *IEEE Trans. Power Electron.*, 9(2):225–231.

[Stumper et al., 2010] Stumper, J.-F., Paulus, D., Landsmann, P., and Kennel, R. (2010). Encoderless field-oriented control of a synchronous reluctance machine with a direct estimator. In *First Symposium on Sensorless Control for Electrical Drives (SLED), 2010*, pages 18–23, Padova, Italy.

[Tomita et al., 1998] Tomita, M., Senjyu, T., Doki, S., and Okuma, S. (1998). New sensorless control for brushless DC motors using disturbance observers and adaptive velocity estimations. *IEEE Trans. Ind. Electron.*, 45(2):274–282.

[Vagati et al., 1997] Vagati, A., Pastorelli, M., and Franceschini, G. (1997). High-performance control of synchronous reluctance motors. *IEEE Trans. Ind. Appl.*, 33(4):983–991.

[Villet et al., 2012] Villet, W. T., Kamper, M. J., Landsmann, P., and Kennel, R. (2012). Evaluation of a simplified high frequency injection position sensorless control method for reluctance synchronous machine drives. In *Proc. IET PEMD 2012*, volume 1, Bristol, UK.

[Wei and Liu, 2012] Wei, M.-Y. and Liu, T.-H. (2012). A high-performance sensorless position control system of a synchronous reluctance motor using dual current-slope estimating technique. *IEEE Trans. Ind. Electron.*, 59(9):3411–3426.

[Xiang and Nasar, 1995] Xiang, Y. Q. and Nasar, S. A. (1995). Estimation of rotor position and speed of a synchronous reluctance motor for servodrives. *IEE Proc. Electr. Power Appl.*, 142(3):201–205.

Errata

Modern synchronous reluctance motors are becoming viable competitors for induction motors in variable-speed drives due to smaller energy losses and simpler structure. In order to operate synchronous motors, information on the rotor position is needed. Position-acquicition methods which do not rely on mechanical sensors are often preferred, since mechanical sensors are expensive and prone to failures. In this thesis, three model-based position-estimation methods are analyzed and experimentally evaluated for synchronous reluctance motors. Since accuracy of the considered estimation methods depends on the equivalent-model parameters, further effort has been put on parameter-estimation methods which can be implemented during normal operation of the drive.

Aalto-DD 86/2014

ISBN 978-952-60-5726-2
ISBN 978-952-60-5727-9 (pdf)
ISSN-L 1799-4934
ISSN 1799-4934
ISSN 1799-4942 (pdf)

Aalto University
School of Electrical Engineering
Department of Electrical Engineering and Automation
www.aalto.fi

BUSINESS + ECONOMY

ART + DESIGN + ARCHITECTURE

SCIENCE + TECHNOLOGY

CROSSOVER

DOCTORAL DISSERTATIONS